TECHNISCHE UNIVERSITÄT WIEN

Diploma Thesis

Optical dipole trap for a caesium Bose-Einstein condensate

submitted in satisfaction of the requirements for the degree of
Diplom-Ingenieur
of the TU Wien, Faculty Physics

Diplomarbeit

Optische Dipol Falle für ein Caesium Bose-Einstein Kondensat

ausgeführt zum Zwecke der Erlangung des akademischen Grades eines
Diplom-Ingenieurs
eingereicht an der Technischen Universität Wien, Fakultät für Physik

von

Maximilian Lerchbaumer

Matr.Nr.: 01127446

unter der Anleitung von

Univ.Prof. Dipl.-Phys. Dr.rer.nat. **Thorsten Schumm**

Univ.Ass. Dipl.-Phys. Dr.rer.nat. **Stephanie Manz**,

Atominstitut
Quantenmetrologie
Technische Universität Wien
Stadionallee 2, 1020 Wien, Österreich

Wien, im Dezember 2018

_____

Betreuer: Professor Thorsten Schumm Maximilian Lerchbaumer

Optische Dipol Falle für ein Caesium Bose-Einstein Kondensat

Abstract

Die besonderen Streueigenschaften von Caesium Atomen, besonders die Einstellbarkeit der Streulänge über magnetisch induzierte Feshbach Resonanzen, machen sie zu einem vielversprechenden Kandidaten um die Phasensensitivität von BEC Materiewelleninterferometern zu verbessern. Sie benötigen aber eine Art von Atomfalle, die nicht auf Magnetfelder angewiesen ist. In dieser dieser Diplomarbeit wird das Design, die Errichtung und die Charakterisierung eines experimentellen Aufbaus für eine optische Dipolfalle auf einem Atomchip präsentiert. Der Atomchip befindet sich in einer sehr kompakten kommerziell erhältlichen UHV Kammer der Firma ColdQuanta. Die Falle wird für die Erzeugung eines Caesium Bose-Einstein Kondensates als eine Quelle für Materiewellen für weitere Experimente verwendet.

Die Falle besteht aus zwei Laserstrahlen mit einer Wellenlänge von 1064 nm welche auf eine Stahltaille von 50 µm fokussiert werden und sich orthogonal kreuzen. Die Strahlen sind um 160 MHz gegeneinander verstimmt um Interferenzeffekte, welche die Atome stören, zu eliminieren. Die Laserleistung P kann kontinuierlich von 0 bis 6 W pro Strahl eingestellt werden, wobei das obere Limit durch die Schadensschwelle der Spiegel gegeben ist, die sich auf dem Atomchip befinden. Aus der Rechnung ergibt sich somit eine Fallentiefe bis zu 450 µK. Die Streurate pro Atom im Punkt höchster Intensität ergibt sich zu $\Gamma = P \cdot 0.8207\,\mathrm{Hz}$. Die Stahlqualität des Fallenstrahls wurde durch eine Messung des sogenannten M^2 Wertes $M^2 = 1.05$ charakterisiert. Es wurde herausgefunden, dass die Temperaturstabilität im Labor die Hauptquelle für Schwankungen der Laserleistung ist . Für Temperaturdrifts von bis zu 3 °C wurden Schwankungen der Leistung von 10% beobachtet. Die Fallengeometrie unter dem Einfluss der Schwerkraft und die daraus resultierenden Fallenfrequenzen wurden simuliert.

Im Weiteren wird darauf eingegangen wie das Experiment aufgebaut wurde wobei auch Sicherheitsvorkehrungen und Wärmemanagement besprochen werden. Zuletzt wird noch ein Ausblick auf den weiteren Verlauf des Experiments gegeben.

Thesis advisor: Professor Thorsten Schumm Maximilian Lerchbaumer

Optical dipole trap for a caesium Bose-Einstein condensate

Abstract

The special scattering properties of caesium atoms, notably the tunability of their scattering length via magnetically induced Feshbach resonances, make them a promising candidate for improving the phase sensitivity in BEC matter-wave interferometry but also require the use of a trapping scheme not reliant on magnetic fields.

In this thesis the design, building and characterization of the experimental setup for an optical dipole trap on an atomchip in a very compact setup using a commercial self-contained UHV chamber by ColdQuanta is presented. The trap will be used for the creation of a caesium Bose-Einstein condensate as a matter-wave source for further experimental directions.

The trap consists of two laser beams with a wavelength of 1064 nm, focussed to a 50 μm waist and crossed orthogonally. The beams are detuned by 160 MHz to eliminate interference effects disturbing the atoms. The laser power P can be continuously adjusted from 0 up to 6 W per beam, limited by the damage threshold of the mirrors on the atomchip yielding a theoretical trap depth up to 450 μK. The scattering rate per atom at the point of highest intensity is given by $\Gamma = P \cdot 0.8207\,\mathrm{Hz}$. The beam quality of the trapping beam has been characterized by a measurement of the M^2 value $M^2 = 1.05$. Temperature instability in the lab was found to be the main source of laser power instability with power fluctuations up to 10% for temperature drifts of about 3 °C. The trap geometry under the influence of gravity and the resulting trap frequencies were simulated.

I will further present how the experiment was set up, including safety precautions and thermal management and a further outlook on the experiment will be given.

Contents

To my parents for their invaluable support, my family for not only teaching me funny poems to put in the epigraphs but also opening my eyes to many aspects of the world I would otherwise have missed, my friends who made my time at university the most fun time yet and Marlene for not only relentlessly dragging me along for experiences I never knew I wanted to have, but also being the best partner I could wish for.

Acknowledgments

I THANK Stephanie Manz, Thorsten Schumm and Benedikt Gerstenecker for teaching me the ropes in the lab and making my time working with them so enjoyable, that I want to continue doing so for a few years to come. I also thank Kjeld Beeks, Jan Welch, Veronika Rosecker and everybody else having lunch with me for the sometimes insightful but all the time funny conversations, you made me feel at home at the institute.

0 Introduction

Matter-wave interferometers are great tools for many metrology applications [1]. The use of caesium as our alkali atom of choice poses some additional challenges compared to other atoms but promises even higher achivable precision by exploiting some of the special properties of caesium atoms. We will trap and laser-cool a cloud of caesium atoms, that have been pumped into the same internal state. We will continue cooling and compressing this cloud until the phase space density is so high, that they all accumulate into the same quantum ground state of an external potential. This is called Bose-Einstein condensation [2]. Compared to other alkali atoms like the rubidium 87 isotope and lithium, caesium poses a special challenge when trying to condense it into a Bose-Einstein condensate (BEC). Generally in caesium the two and three-body inelastic scattering is exothermic and the scattering rates are high. This leads to a heating of the atom cloud when higher densities are reached. Pumping the atoms into the absolute ground state $|F = 3, m_f = 3\rangle$ suppresses

all inelastic two-body collisions, which are endothermic in this state, at low enough temperatures. This state is a high-field-seeking state with respect to a magnetic field and can therefore not be captured magnetically [3]. Unfortunatly three-body inelastic scattering is still not supressed. In this process two atoms bond into a molecule and the third atom gets two thirds of the molecules binding energy [4]. This release of energy and subsequent heating prohibits the formation of a Bose-Einstein condenstate [5]. To overcome this, another property of caesium atoms can be exploited. A homogeneous magnetic field can be applied to continuously tune the s-wave interaction strength from attractive to repulsive [6]. This makes it not only possible to condense the cloud into a BEC [7] but also to potentially greatly improve the quality of ensuing measurements. To be able to tune the magnetic field as a free parameter and because magnetic traps cannot be used for a high-field-seeking state, the need for a trapping scheme arises that is not dependent on magnetic fields. A dipole trap uses only the interaction of far red, or in rarer cases blue, detuned laser light with the atoms induced dipole moment to confine atoms in arbitrary states, therefore leaving the magnetic field as a free parameter. In this thesis I will present how I designed and built the laser and parts of the experimental setup to be used for dipole trapping in our caesium matter-wave interferometer.

Ein Metterschling

mit flauen Bügeln

log durch die Fuft.

1

Dipole Trapping

To create an ultra-cold cloud of neutral atoms in a vacuum chamber, one has to trap the atoms in some kind of potential minimum. The two possible methods of trapping are magnetic traps and dipole traps. For reasons that I will explain later in this thesis we need our atoms to be in a high field seeking state with respect to magnetic fields. This makes them unsuitable for magnetic trapping schemes. This leaves us with our method of choice: dipole trapping.

This way of trapping atoms exploits the interaction between the dipole moment induced by the electric field of a laser beam and the beams intensity gradient. For the case of red-detuned light, said interaction causes the atoms to be drawn to the highest intensity of laser light. The two most important experimental parameters of a dipole trap, balancing atom lifetime and trap depth, are the detuning from the closest atomic reso-

nances Δ of the laser light and the intensity I of the laser beam. In the following treatment we will see, that the attractive potential U scales with I/Δ, whereas the scattering rate Γ scales with I/Δ^2.

Because of this fact dipole traps mostly operate in a far red-detuned regime, to minimise scattering, and with high powered lasers to account for the weakening of the potential when detuning.

1.1 Classical treatment

In this section I will summarize the key points of the general theory of trapping neutral atoms by means of the dipole interaction. I will follow the concise treatment found in "Optical Dipole Traps for Neutral Atoms"[8].

A single atom in laser light will be polarized by the lasers electric field $\vec{E} = \hat{e}E(\vec{r})exp(-i\omega t) + c.c.$. Where $\hat{e}$ is the unit polarization vector. This polarization $\vec{p} = p(\vec{r})exp(-i\omega t) + c.c.$ can be approximated by

$$\vec{p} = \alpha\vec{E}\,, \tag{1.1}$$

where α is the complex polarizability of the atom. When averaged over time (denoted by angle brackets) the interaction between this polarization and the electric field leads to a potential

$$U_{dip}(r) = \frac{1}{2}\langle\vec{p}\vec{E}(r)\rangle = \frac{1}{2}\,\mathrm{Re}(\alpha)\langle\vec{E}\vec{E}(r)\rangle = \frac{1}{2}\,\mathrm{Re}(\alpha)\langle E^2(r)\rangle = \frac{1}{2\varepsilon_0 c}\,\mathrm{Re}(\alpha)I(r)\,, \tag{1.2}$$

using $I = 2\varepsilon_0 c|E^2|$. Here ε_0 is the dielectric constant and c the speed of light. We now see that the potential is dependent on the intensity of the laser beam and the real part of the complex polarizability, which describes the in-phase component of the dipole oscillations.

The power absorbed by the atoms on the other hand is given by

$$P_{abs} = \langle\dot{\vec{p}}\vec{E}\rangle = \frac{\omega}{\varepsilon_0 c}\,\mathrm{Im}\,\alpha I(r)\,, \tag{1.3}$$

with ω being the frequency of the electric field. The corresponding scattering rate is

$$\Gamma_{sc}(r) = \frac{1}{\hbar\varepsilon_0 c}\,\mathrm{Im}(\alpha) I(r)\,. \tag{1.4}$$

It is again dependent on the intensity and the imaginary part of the polarizability, describing the out-of-phase part of the dipole oscillations.

Now we need to find an expression for the polarizability α. For D lines of alkali atoms (as seen in figure 1.1) and intensities far from saturation we can use a classical approximation which agrees to a few percent with the exact result [8]. We assume the electron (mass m_e, charge e) to be bound elastically to the core with an oscillation eigenfrequency ω_0 corresponding to the optical transition frequency. Damping results from the dipole radiation of the oscillating electron, which can be related to Larmor's formula for power radiated by an accelerated charge. Putting everything together and solving the differential equation for a damped driven harmonic oscillator $\ddot{x} + \Gamma_w \dot{x} + \omega_0^2 x = -eE(t)/m_e$ in a calculation, that is beyond the scope of this section [8], gives

$$\alpha = \frac{e^2}{m_e} \frac{1}{\omega_0^2 - \omega^2 - i\omega\Gamma_w}\,, \tag{1.5}$$

where

$$\Gamma_w = \frac{e^2}{m_e} \frac{\omega^2}{6\pi\varepsilon_0 c^3} \tag{1.6}$$

is the classical damping rate due to the radiative energy loss. Substituting $\frac{e^2}{m_e} = \Gamma_w 6\pi\varepsilon_0 c^3/\omega^2$ and introducing the on-resonance damping rate $\Gamma = \Gamma_{w_0} = (\omega/\omega_0)^2\Gamma_w$ we get

$$\alpha = 6\pi\varepsilon_0 c^3 \frac{\Gamma\omega_0^2}{\omega_0^2 - \omega^2 - i(\omega^3/\omega_0^2)\Gamma}\,. \tag{1.7}$$

Using this result in equations (1.2) and (1.4) we get

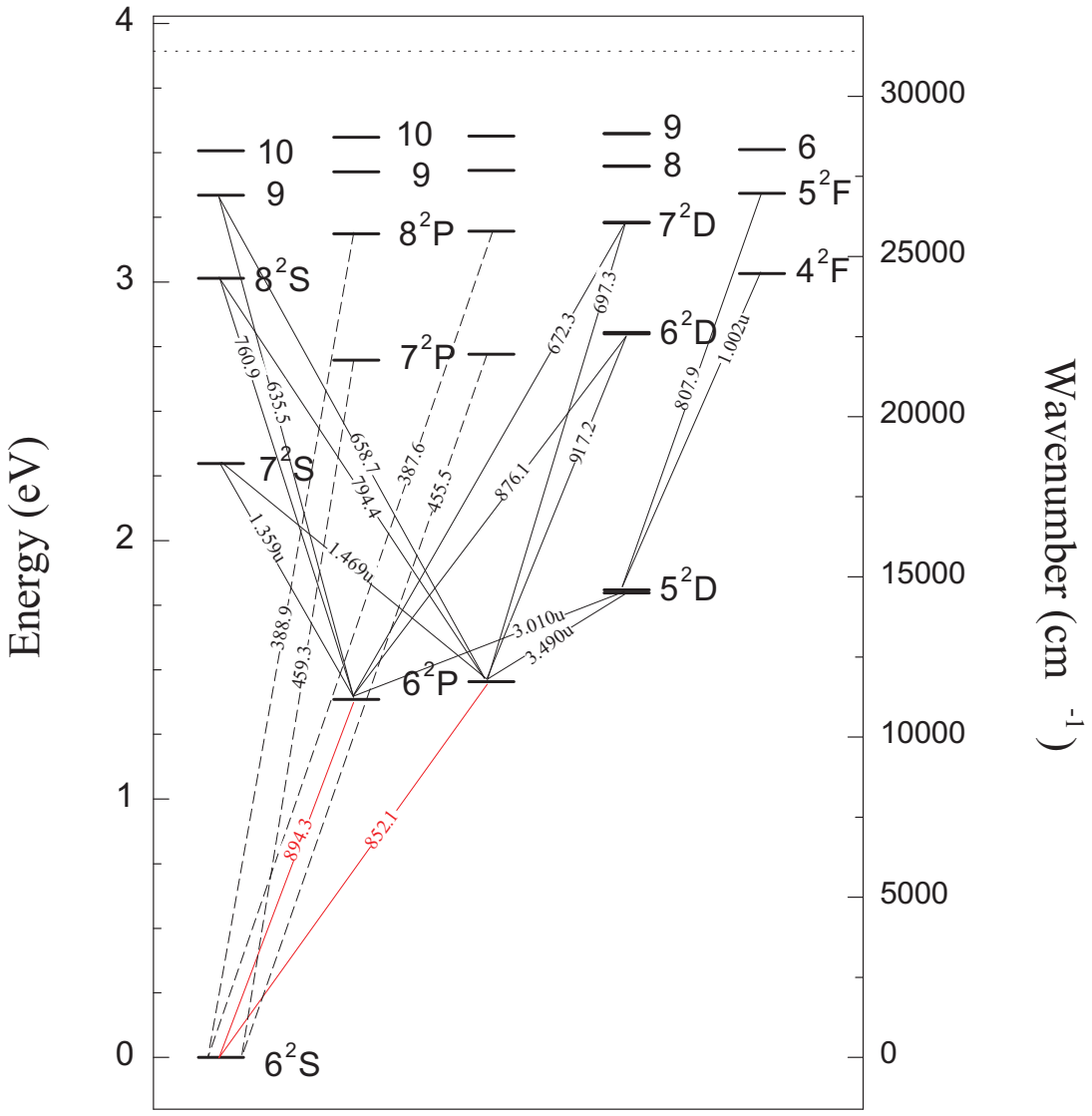

Figure 1.1: Grotrian diagram of the caesium transitions taken from [9]. The two lines marked red are the $D1$ and $D2$ transitions

$$U_{dip}(\vec{r}) = \frac{3\pi c^2}{2\omega_0^3}\left(\frac{\Gamma}{\omega_0 - \omega} + \frac{\Gamma}{\omega_0 + \omega}\right) I(\vec{r})\,, \tag{1.8}$$

$$\Gamma_{sc}(\vec{r}) = \frac{3\pi c^2}{2\hbar\omega_0^3}\left(\frac{\omega}{\omega_0}\right)^3\left(\frac{\Gamma}{\omega_0 - \omega} + \frac{\Gamma}{\omega_0 + \omega}\right)^2 I(\vec{r})\,. \tag{1.9}$$

If the laser is tuned close to resonance so that the detuning $\Delta = \omega - \omega_0$ is much smaller than the resonant frequency $|\Delta| << \omega_0$ we can neglect the counter rotating term $\Gamma/(\omega_0 + \omega)$ with its resonance at $\omega = -\omega_0$. We obtain

$$U_{dip}(\vec{r}) = \frac{3\pi c^2}{2\omega_0^3}\frac{\Gamma}{\Delta} I(\vec{r})\,, \tag{1.10}$$

$$\Gamma_{sc}(\vec{r}) = \frac{3\pi c^2}{2\hbar\omega_0^3}\left(\frac{\Gamma}{\Delta}\right)^2 I(\vec{r})\,. \tag{1.11}$$

This is called the *rotating wave approximation*. We now see that the potential indeed is attractive for 'red' detuning $\Delta < 0$ and that the potential minimum is found at the place of highest intensity. For 'blue' detuning $\Delta > 0$ the potential repels atoms out of high intensity areas, creating a minimum at the place of lowest intensity.

1.2 Multi level atoms

Compared to the treatment in the last section, in which we only looked at two-level atoms, I will now describe the Cs atom as a multi-level one. To investigate how the other atomic transitions influence the potential, we will treat the laser light as a perturbation in the atoms Hamiltonian. For the interaction Hamiltonian $\mathcal{H}_1 = \hat{\mu}\vec{E}$, where $\hat{\mu} = -e\vec{r}$ is the electric dipole operator, the second-order time-independent perturbation theory yields the following result for the energy shift:

$$\Delta E_i = \sum_{i \neq j} \frac{|\langle j| \mathcal{H}_1 |i\rangle|^2}{\mathcal{E}_i - \mathcal{E}_j}, \tag{1.12}$$

where $\mathcal{E}$ are the unperturbed energies. Now we will use the so-called *dressed state* picture. The ground state atom has zero internal energy but the field energy is $n\hbar\omega$ depending on the number n of photons. This gives a total energy of $E_i = n\hbar\omega$. When the atom absorbs a photon from the field n decreases by one and the atoms energy becomes $\hbar\omega_0$. The total energy now is

$$E_j = \hbar\omega_0 + (n-1)\hbar\omega = -\hbar(\omega - \omega_0) + n\hbar\omega = -\hbar\Delta_{ij} + n\hbar\omega \tag{1.13}$$

with $\mathcal{E}_i - \mathcal{E}_j = \Delta_{ij}$.

For a simple two level atom and using the rotating wave approximation the expression 1.12 then gives

$$\Delta E = \pm \frac{|\langle e| \mu |g\rangle|^2}{\Delta} |E|^2 = \pm \frac{3\pi c^2}{2\omega_0^3} \frac{\Gamma}{\Delta} I \tag{1.14}$$

for the ground and excited state (upper and lower sign, respectively). Here we used that $I = 2\varepsilon_0 c|E|^2$ and

$$\Gamma = \frac{\omega_0^3}{3\pi\varepsilon_0 \hbar c^3 |\langle e| \mu |g\rangle|^2}. \tag{1.15}$$

We now see, that the presence of the light field shifts our ground and excited state energy. For 'red' detuned light the ground state energy is lowered and the excited states energy increased. This is known as the *light shift* or *AC Stark shift*. Interestingly the shift of the ground state energy corresponds exactly to the result derived earlier 1.10. For low saturation the atom resides in the groundstate most of the time and we can interpret the light-shifted ground state as the relevant potential for the motion of atoms.

For multi-level atoms we have to use the dipole matrix elements $\mu_{ij} = \langle e_j| \mu |g_i\rangle$ between different electronic ground states $|g_i\rangle$ and excited states $|e_j\rangle$. This matrix element can be written as $\mu_{ij} = c_{ij}||\mu||$ with the reduced matrix element $||\mu||$ and the real transition coefficient c_{ij}. With this the energy shift for a multi-level

atom ground state can be written as

$$\Delta E_i = \frac{3\pi c^2 \Gamma I}{2\omega_0^3} \sum_j \frac{c_{ij}^2}{\Delta_{ij}} \,. \tag{1.16}$$

We see, that in order to get the energy shift for a multi-level atom ground state we just sum the contributions of the excited states $|e_j\rangle$ an weigh them with their respective line strengths c_{ij}^2 and detunings Δ_{ij}.

1.3 Cs atoms in a focused Gaussian beam

The geometry of the potential created by a single focused Gaussian laser beam is only dependent on its intensity profile. Expressed in polar coordinates with x pointing in the direction of the beam and r being the distance to the beams centre, the intensity is given by

$$I(r,x) = \frac{2P}{\pi w(x)^2} exp\left(-(2r^2/w(x)^2) \right) . \tag{1.17}$$

Where the waist size $w(x)$ is half the $1/e^2$ diameter of the laser beam

$$w(x) = w_0 \left(1 + \left(\frac{\lambda x}{\pi w_0^2} \right)^2 \right)^{1/2} . \tag{1.18}$$

Here w_0 is the minimum beam waist size in the focal point. Now we will use 1.8 and 1.9 with our knowledge that we have to sum the different contributions of the excited states in a multi-level atom with their respective line strengths and detunings (1.16). For Cs the two relevant transitions are the $D_1(6^2S_{1/2} \rightarrow 6^2P_{3/2})$ and $D_2(6^2S_{1/2} \rightarrow 6^2P_{1/2})$ transition. All other transitions have such high resonant frequencies ω_0, that the $1/\omega_0^3$ term makes them negligible regardless of their line strengths.

Inserting the values for Caesium using linear polarized light from table 1.1 and taking into account both the line strength factors of $\frac{1}{3}$ and $\frac{2}{3}$ for $\omega_0 = D_1$ and $\omega_0 = D_2$ respectively we get a formula for our trap potential in Joules.

m_{Cs}	$2.20694650 \cdot 10^{-25}$kg	Mass of the Cs atom
Γ_{D1}	$2\pi \cdot 4.5612 \cdot 10^{6}$Hz	Linewidth of the D_1 line
Γ_{D2}	$2\pi \cdot 5.2227 \cdot 10^{6}$Hz	Linewidth of the D_2 line
D_1	$2\pi * 335.116048807 \cdot 10^{12}$Hz	D_1 line angular frequency
D_2	$2\pi * 351.72571850 \cdot 10^{12}$Hz	D_1 line angular frequency

Table 1.1: Table of Cs specific values [10]

$$U_{dip}(r,x) = \frac{-I(r,x)\pi c^2}{2}\left(\frac{\Gamma_{D1}}{D_1^3}\left(\frac{1}{D_1-\omega_L}+\frac{1}{D_1+\omega_L}\right)+\frac{2\Gamma_{D2}}{D_2^3}\left(\frac{1}{D_2-\omega_L}+\frac{1}{D_2+\omega_L}\right)\right) \tag{1.19}$$

where $\omega_L = 2\pi c/\lambda$ is the laser frequency, c the speed of light in vacuum and λ the lasers wavelength.

The expression for the scattering rate $\Gamma_{Scattering}$ is

$$\Gamma_{Scattering}(\omega_L) = \frac{\pi c^2 I_{max}}{2\hbar}\left[\frac{\Gamma_{D1}^2}{D_1^3}(\frac{\omega_L}{D_1})^3(\frac{1}{D_1-\omega_L}+\frac{1}{D_1+\omega_L})^2+\frac{2\Gamma_{D2}^2}{D_2^3}(\frac{\omega_L}{D_2})^3(\frac{1}{D_2-\omega_L}+\frac{1}{D_2+\omega_L})^2\right]. \tag{1.20}$$

Cs specific values are found in table 1.1

Expressions for the trap frequencies can be gained from Taylor expansions of $U_{dip}(r=0,x)=U_x(x)$ and $U_{dip}(r,x=0)=U_r(r)$ at $x=r=0$ and comparing with the potential of the harmonic oscillator $U_{harm}(x)=\frac{1}{2}\omega^2x^2$. The angular frequency is $\omega_{harm}=2\pi\nu$ with the trap frequency ν. Our experiment uses two beams crossed at a 90 degree angle. We now change from polar coordinates to Cartesian ones with z being the direction perpendicular to both beams. Let us now denote the potential of both beams in the direction of one beam with V_x and the potential perpendicular to both beams at their intersection with V_z. Expressing V_x and V_z by using U_x and U_r we get $V_z(z)=2U_r(r\to z)$ and $V_x(x)=U_r(r\to x)+U_z(z\to x)$. Doing the Taylor expansion of V_z and V_x and comparing with the harmonic oscillator we get

$$\nu_z = \sqrt{\frac{-U_{min}}{m_{Cs}w_0^2}}/(2\pi) \tag{1.21}$$

for the trap frequency in z direction and

$$\nu_{xy} = \sqrt{\frac{-U_{min}}{m_{Cs}}\left(\frac{1}{w_0^2} + \frac{\lambda^2}{\pi^2 w_0^4}\right)}/(2\pi) \tag{1.22}$$

for the trap frequency in either x or y direction, with $U_{min} = 2U_{dip}(0,0)$ being the minimum of the dipole potential of two crossed beams.

Since the trapping potential is approximately harmonic around the trap minimum we can assign it a characteristic frequency. This frequency called the trap frequency tells us not only with which frequency we expect the cloud of atoms to oscillate in the trap but also tells us about its shape. Higher trap frequencies tell you that the trap is more confined and vice versa. When loading from one trap to another it is important, that the trap frequencies of both traps are at least similar. If that is not the case you either loose atoms because the trap you are loading into is smaller than the original one (the new trap frequency is a lot higher) or the atom cloud heats up because it can suddenly expand and is therefore shaken up (new trap frequency is too low).

1.4 The effect of gravity

In our set-up the force of gravity is pointing in the z - direction (perpendicular to both beams). To account for its effect on our trapping potential we add a term

$$U_{grav}(z) = -g m_{Cs} z \tag{1.23}$$

to the potential of the two crossed laser beams, with $g = 9.81\,\mathrm{m\,s^{-2}}$ being the gravitational acceleration of the earth.

Since the atoms in our experiment are in a high field seeking state this effect can be counteracted with a magnetic field gradient given by

$$B_{grad} = \frac{m_{Cs} g}{2\pi\hbar\mu_B g_F m_F}\,. \tag{1.24}$$

The state we use in our experiment is the $F = 3$, $m_F = 3$ state. Its hyperfine Landé g factor is $g_F = -0.35\,\mathrm{MHz\,G^{-1}}$. Inserting all values into the equation yields $B_{grad} = 31.1\,\mathrm{G\,cm^{-1}}$.

Er wurde einem Computer entnommen,

dem war was durcheinander gekommen:

2

Simulation

I SIMULATED A Cs DIPOLE TRAP, based on the results from the last chapter, to decide what laser wavelength and minimum beam waist would meet our experimental requirements best and also to decide how powerful the laser would have to be.

In the following trap depth refers to the depth of the potential well in the middle of the trap. Without gravity, meaning with the magnetic field gradient discussed in 1.4 on, the trap depth is about half the absolute minimum of the trapping potential $V_x(x)$ (a rather optimistic approximation). This is due to the fact, that the atoms could still move in the direction of one of the beams and therefore be lost (see 2.1a). With gravity, the trap depth is limited in the z-direction because the potential will be tilted (see Figure 2.1b). In this case the trap depth is the difference of the local minimum and maximum of the potential $V_z(z) - U_{grav}(z)$ (see

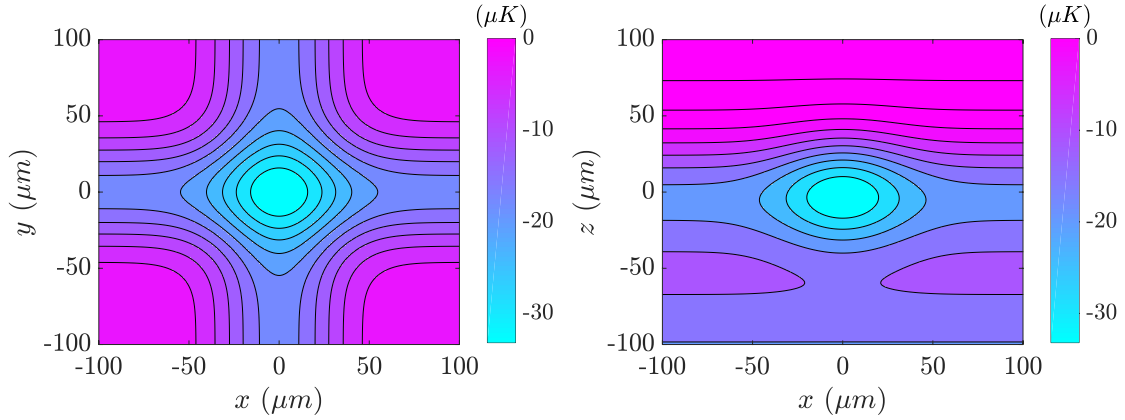

(a) Top view **(b)** Side view

Figure 2.1: Equipotential lines of the trap potential in the xy plane 2.1a and on the xz plane 2.1b (looking directly into one beam). In the top view you can see, that the atoms can escape in the direction of the beam. I estimated the trap depth (first closed equipotential line) in x or y direction to be roughly half of the total depth. In the side view you can see the effect of gravity opening the trap on the bottom. For this case I calculated the trap depth as explained in Figure 2.2. The simulation parameters were: $P = 0.25\,\mathrm{W}$, $w_0 = 50\,\mu\mathrm{m}$ and $\lambda = 1064\,\mathrm{nm}$.

Figure 2.2).

One of the most important factors, concerning the dipole trap, for our BECs lifetime is the scattering rate $\Gamma_{Scattering} \propto I/\Delta^2$. Any atom that scatters a photon can be considered as having gained enough energy to be able to leave the trap. On its way out of the trap it can hit other atoms, heating the BEC and further decreasing its lifetime. The scattering rate has to be balanced with the strength of the potential $U \propto I/\Delta$ so that trapping can still be achieved with sensible laser power for experimental feasibility.

For this purpose I calculated the depth of the trap, with and without gravity compensation, and the scattering frequency dependent on the laser wavelength for a laser power of $P = 100\,\mathrm{mW}$ and a minimum beam waist $w_0 = 50\,\mu\mathrm{m}$ (figure 2.4). Trap depth, together with scattering rate, is linearly dependent on P (see equation 1.17)

To help decide on the beam waist to be used I plotted the beam waist versus the trap depth and trap frequency (see Figure 2.5).

From these simulations we concluded that we would use a beam waist of $w_0 = 50\,\mu\mathrm{m}$, a laser with wavelength $\lambda = 1064\,\mathrm{nm}$ and enough power to reach $P = 6\,\mathrm{W}$ per trap beam. The scattering rate per atom at the point of highest intensity is given by $\Gamma = P \cdot 0.8207\,\mathrm{Hz}$. A summary of these values can be found in table 2.1.

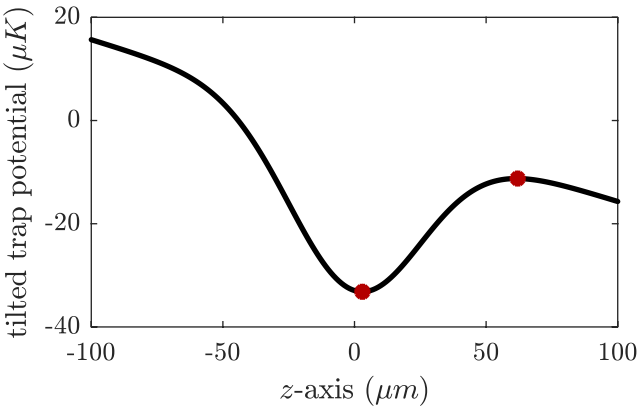

Figure 2.2: Plot of the potential along the z axis. It is tilted by the effect of gravity. To calculate the trap depth in z direction I determined the local maxiumim and minimum (red dots in the plot) and set their potential difference to be the trap depth. The simulation parameters were: $P = 0.25\,\mathrm{W}$, $w_0 = 50\,\mu\mathrm{m}$ and $\lambda = 1064\,\mathrm{nm}$

.

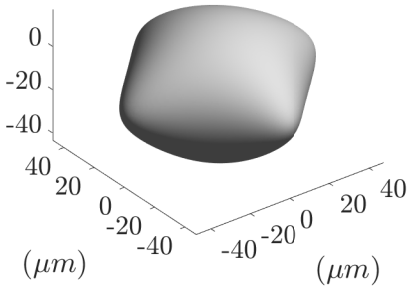

(a) 13 μK

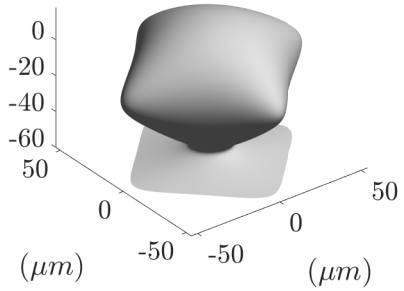

(b) 14 μK

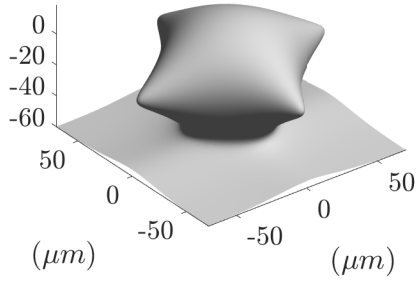

(c) 15 μK

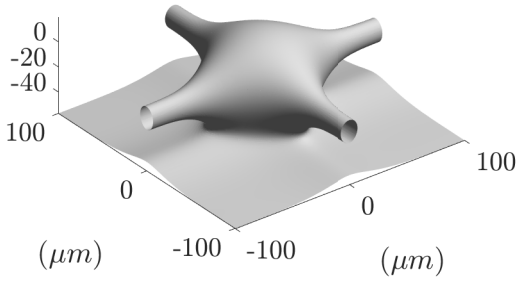

(d) 16 μK

Figure 2.3: This figure shows different equipotential surfaces of the trap potential. The point $(0, 0, 0)$ is where the two laser beams meet. In 2.3a you can see that atoms with a temperature of $13\,\mu\mathrm{K}$ and lower would still be held in the trap, but the trap is shifted by about $15\,\mu\mathrm{m}$ in z direction. For $14\,\mu\mathrm{K}$ 2.3b you can see, that atoms would already fall out at the bottom of the trap and at $16\,\mu\mathrm{K}$ 2.3d the atoms could also escape along the laser beams. The simulation parameters were: $P = 0.25\,\mathrm{W}$, $w_0 = 50\,\mu\mathrm{m}$ and $\lambda = 1064\,\mathrm{nm}$.

Beam waist w_0	50 µm
Laser wavelength λ	1064 nm
Scattering rate per watt Γ/P	0.8207 Hz
Trap depth per watt D_x/P	70 µK

Table 2.1: This table summarizes the chosen parameters for the dipole trap

This beam waist yields trap frequencies in a range that most closely fits the trap frequencies of the magnetic trap before. The wavelength is a good trade-off between scattering rates being low and the laser power needed staying in a sensible limit. Also 1064 nm lasers are readily available. We expect to reach trap depths of a few hundred micro kelvin needing laser powers of one to two watt per beam.

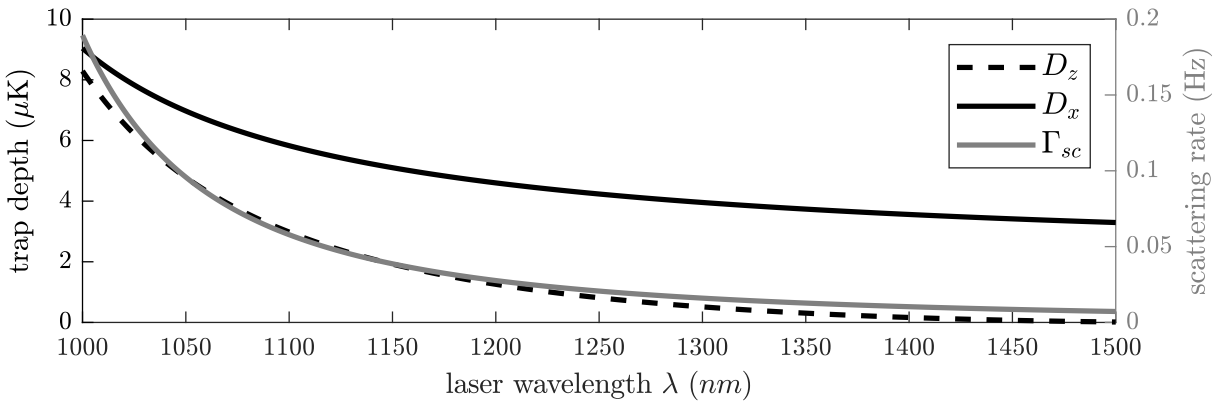

Figure 2.4: Depth of the trapping potential with (D_z) and without (D_x) the influence of gravity and scattering rate at the point of highest intensity Γ_{sc} as a function of laser wavelength. Laser power is $P = 100\,\mathrm{mW}$ and beam waist $w_0 = 50\,\mu\mathrm{m}$.

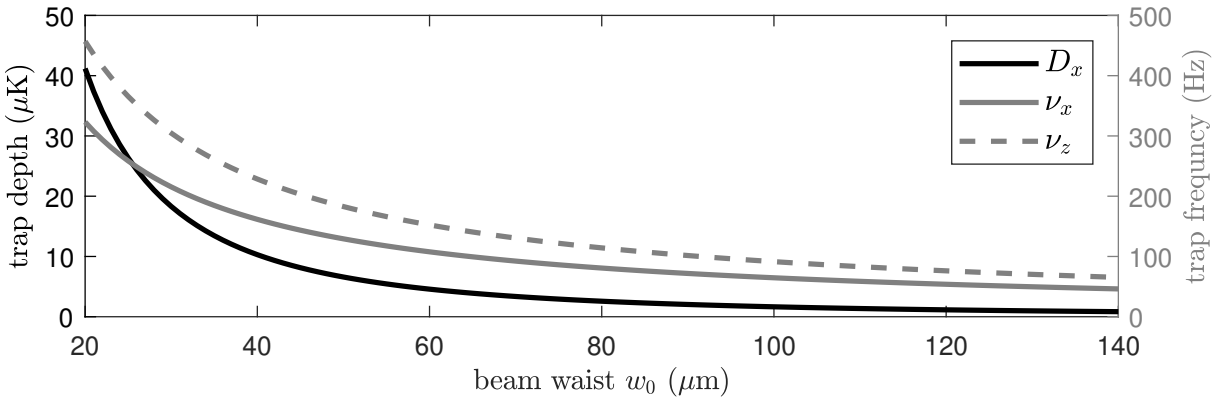

Figure 2.5: Depth of the trapping potential without the influence of gravity (D_x) and trap frequency in x (ν_x) and z (ν_y) direction as a function of beam waist size. Note that the trap frequency does not scale with P like the depth but with $\sqrt{P}$ which makes this plot slightly less useful than Figure 2.4. Laser power is $P = 100\,\mathrm{mW}$ and wavelength $\lambda = 1064\,\mathrm{nm}$.

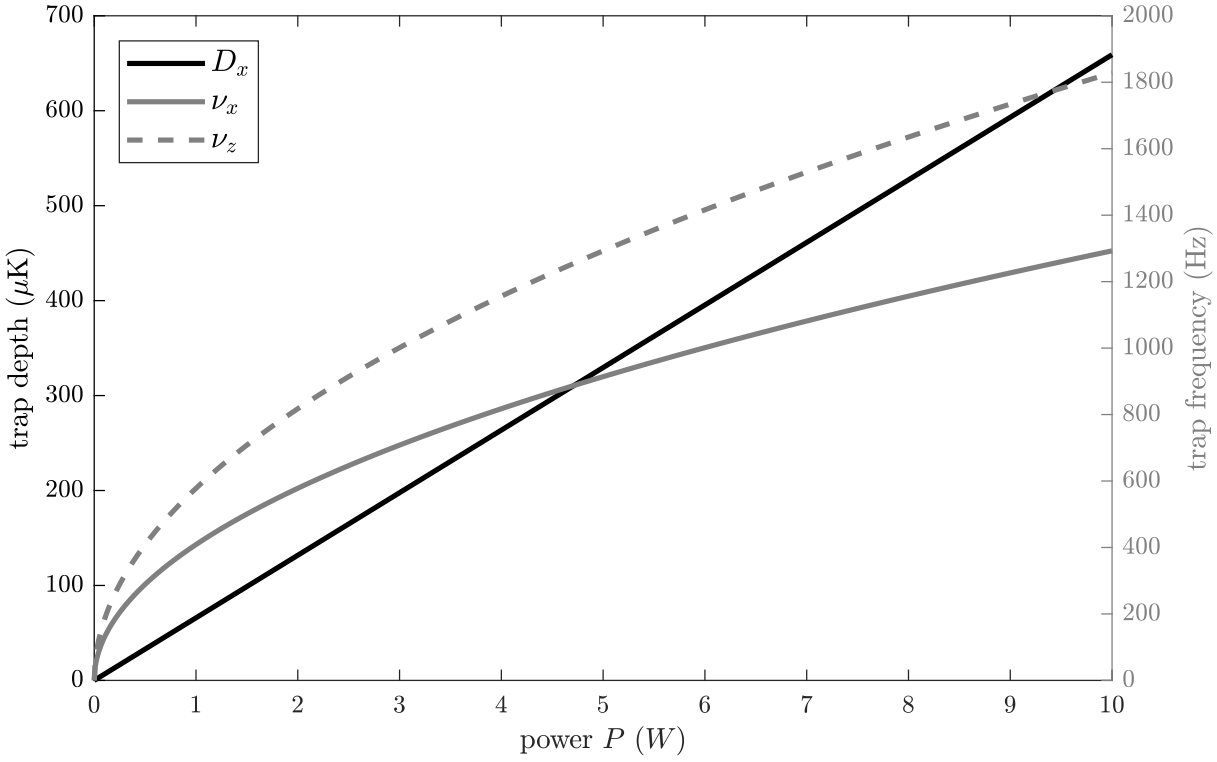

Figure 2.6: Trap depth without gravity D_x and trap frequency ν in x and z direction plotted against laser power P, where P is the power per beam. Beam waist is $w_0 = 50\,\mu\mathrm{m}$ and wavelength is $\lambda = 1064\,\mathrm{nm}$.

irgendein Rädchen,

irgendein Drähtchen,

3

Setup Design

With all important values fixed, we started to design the laser setup.

We know that two crossed laser beams with the same polarization and similar frequency will form a standing wave in a lattice-like interference pattern[11] which would make the trapping potential non-harmonic and ruin the trap. Even worse, if the beams are not perfectly in phase, form a slow moving version of such a pattern and transport atoms out of the trap like a conveyor belt. One solution for counteracting this is splitting the original laser beam in two and detuning one beam by 80 MHz up and one by 80 MHz down so that the interference pattern moves faster than the atoms can notice it. The detuning is realized using two acousto-optic modulators (AOMs). One AOM is aligned so that the first order deflection (frequency shifted up) is strongest and one so that the minus first order (frequency shifted down) is strongest. Using two AOMs we

can also modulate the intensity of each beam separately. After modulation both beams are coupled into polarization maintaining fibres, so that the laser system can be built on a separate optical table.

For deciding what the lasers maximum output power should be we calculated the power needed for two beams with a power of 5 W at the position of the atoms in the vacuum system. These beams are prepared for the dipole trap. The power together with the laser beams waist size is below the damage threshold of $10^9\,\mathrm{W\,cm^{-2}}$ of the mirrors on the chip [14]. A bit of extra overhead was added for potentially generating a third beam for generating double-well potential later on. With expected worst case losses of 40% at the AOMs and couplers the minimum laser power per beam was 14 W ($14 * 0.6^2 = 5.04$). So we decided to use a 50 W laser. This gives us a estimated upper limit of 9 W per beam with the maximum expected losses. This estimate is rather conservative as the experiment will probably never need this much power. Other requirements for the laser were reasonably low noise, a small line width and high power stability.

The fibres needed to be polarization maintaining, since polarization stability is essential to the trapping potential. Also, the fibre couplers had match the numerical aperture of the fibres. Furthermore, both, fibres, couplers, and AOMs needed to be able to withstand around 20 W of laser power.

3.1 General description of the set-up

We chose to build the setup on a 60 cm by 90 cm optical table. Although it would have been possible to build it on a more compact table, this size fitted our room very well and larger spacing between optical components makes it easier to service the optical components should the need arise. The layout is shown in figure 3.1. Right after the laser head we placed a half-wave plate and a beam splitter (PBS1 in the figure) with one path going to the experiment and one into a beam dump. The beam splitter is used to regulate the laser power for alignment, since the lowest possible output power of the laser is still around 200 mW which is not really necessary for most alignment tasks (except aligning with high power absorption when misaligned, for example the pinhole filter) and already powerful enough to quickly damage eyes. After this we use a pinhole assembly to remove any non-Gaussian modes of the laser beam (more on the pinhole assembly in section 4.3). Now the

beam is split into two equally strong parts using another half-wave plate and beam splitter (PBS2). The two beams are modulated by one AOM each. Each zeroth order beam is dumped into a high power beam dump using a "D-Shaped Pickoff Mirror". Then each modulated beam is aligned into a polarization maintaining fibre using a half-wave plate for aligning the polarization of the beam with the slow axis of the fibre.

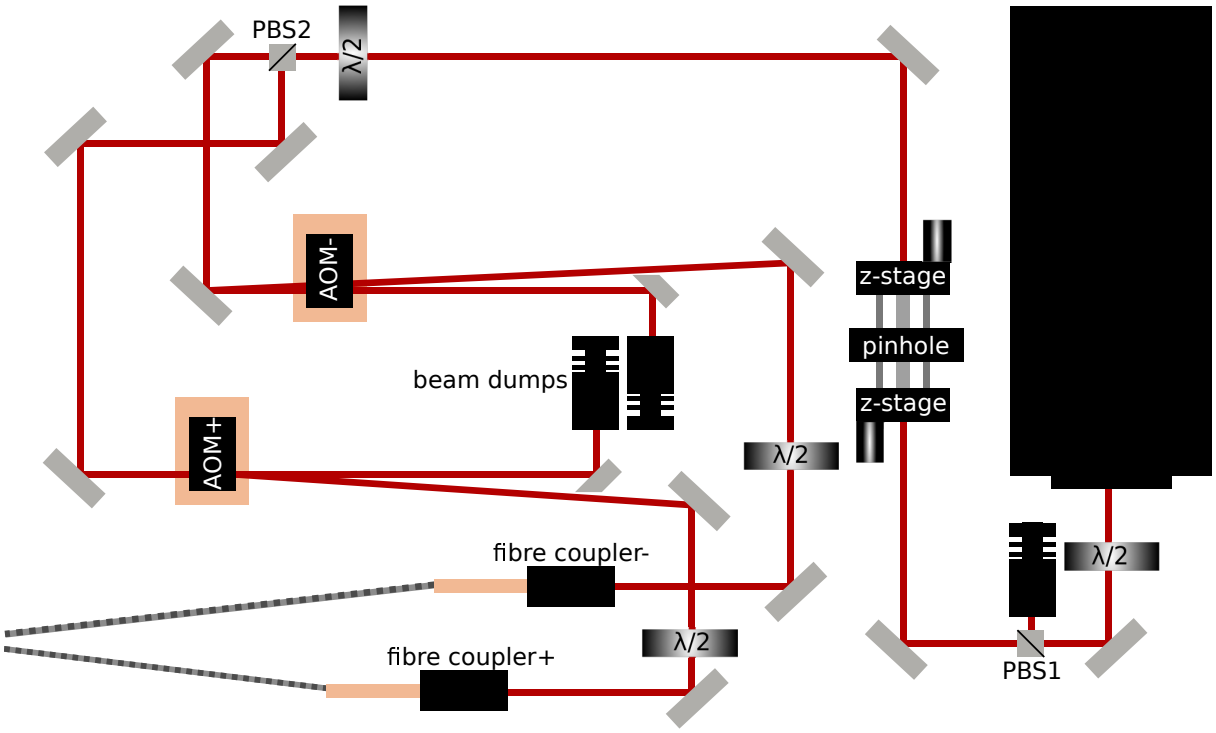

Figure 3.1: Schematic of the Laser set-up.

The experiment side of the setup is shown in figure 3.3. I designed it such that it would take up the least amount of space possible since one goal of the experiment is to be as compact as possible. After the beam leaves the fibre coupler collimated, it is focused by a lens mounted in a *xy*-stage. The stage is in turn mounted to the coupler using cage rods (see figure 3.4). This gives an adjustability of 5 mm in x and y and 1 cm in z direction. The lens has a focal length of 25 cm. Together with the coupler producing a measured $1/e^2$ beam radius of 1.6 mm, this focuses the beam to a waist of 53 µm which is very close to the desired 50 µm (again waist is half $1/e^2$ diameter).

The focal length of the lens allows us to place the lens on the table opposed to having it mounted right next to the glass cell and leaves us with enough space for two mirrors, simplifying alignment. On the other

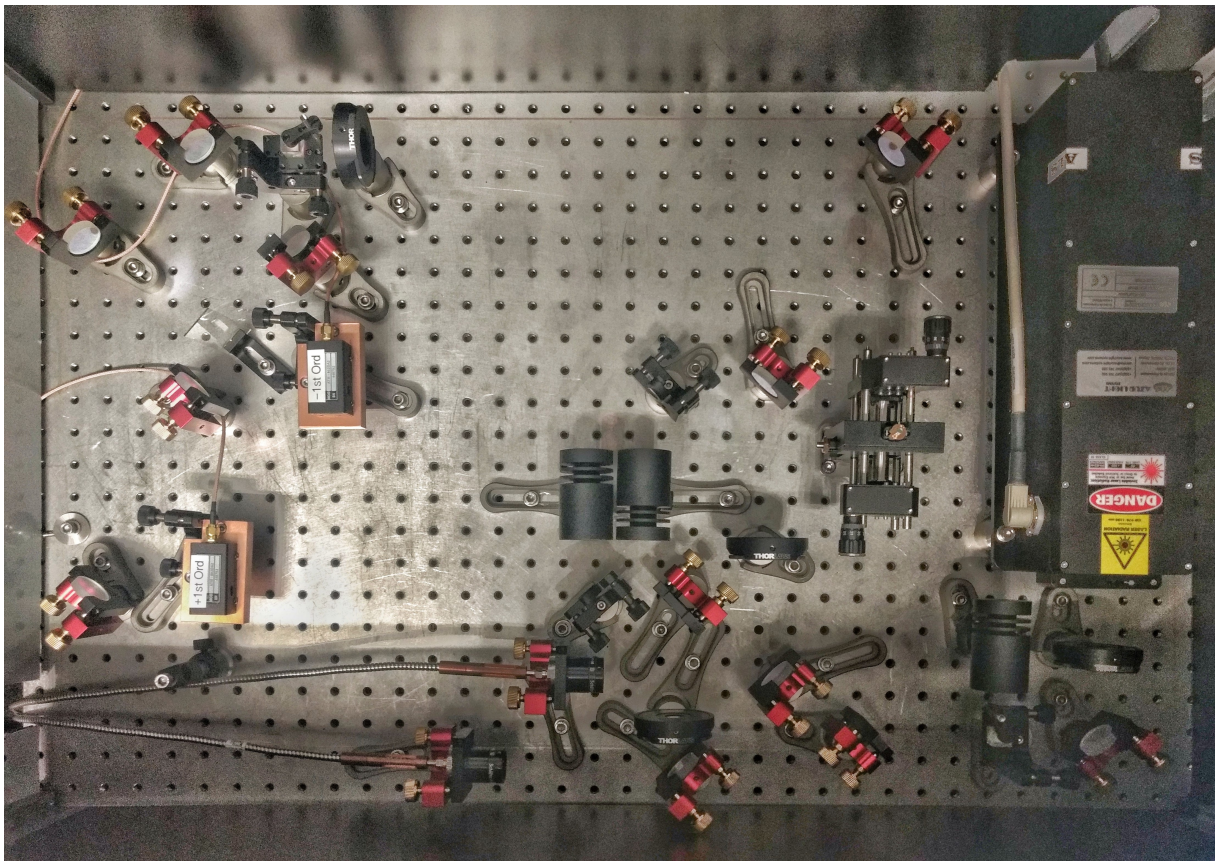

Figure 3.2: Photograph of the Laser setup

hand it is also short enough as to not waste space with a needlessly long beam path. Moving the lens mount on the cage rods we can move the focal point of the lens to be as close to the middle of the chip as possible. This can be checked by comparing the beam diameter before and after the glass cell at the exact same distance to the cell. If they are the same, the focal point must be right in the middle of the cell. A second way to check alignment will be the shape of the cloud of trapped atoms. The xy-stage is used to correct any misalignment between coupler and lens. A rendering of the chip can be seen in figure 3.5.

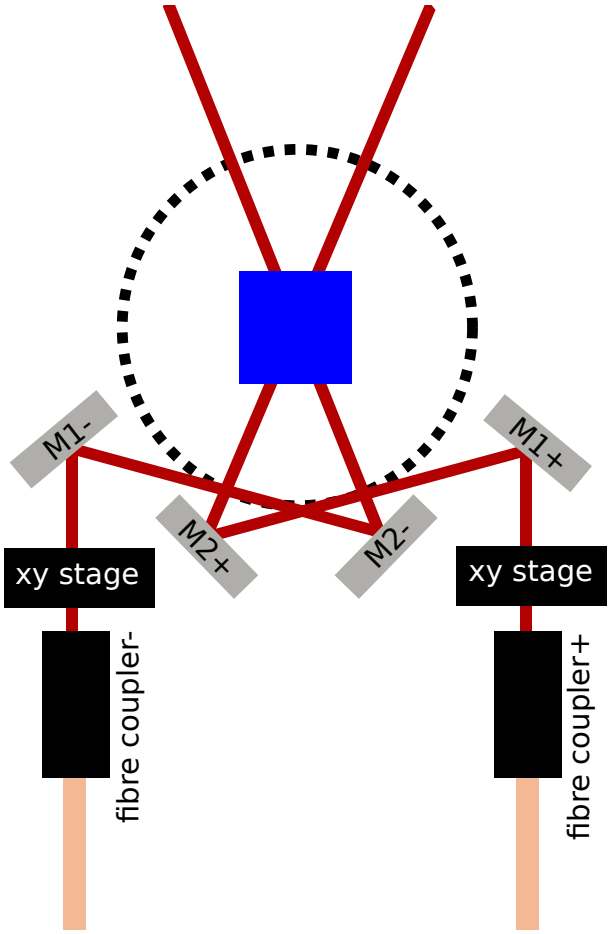

Figure 3.3: Schematic of the laser setup near the chip. Mirrors M2+ and M2- are mounted on posts tilted by 12 degrees. The lenses are mounted in the xy-stages. The dotted circle shows the hole in the mounting plate in which the glass chamber sits and the blue square marks the position of the chip. The chip is about 4 cm above the plane in which the beam leaves the couplers. The path the beams take underneath the chip can be seen in figure 3.5

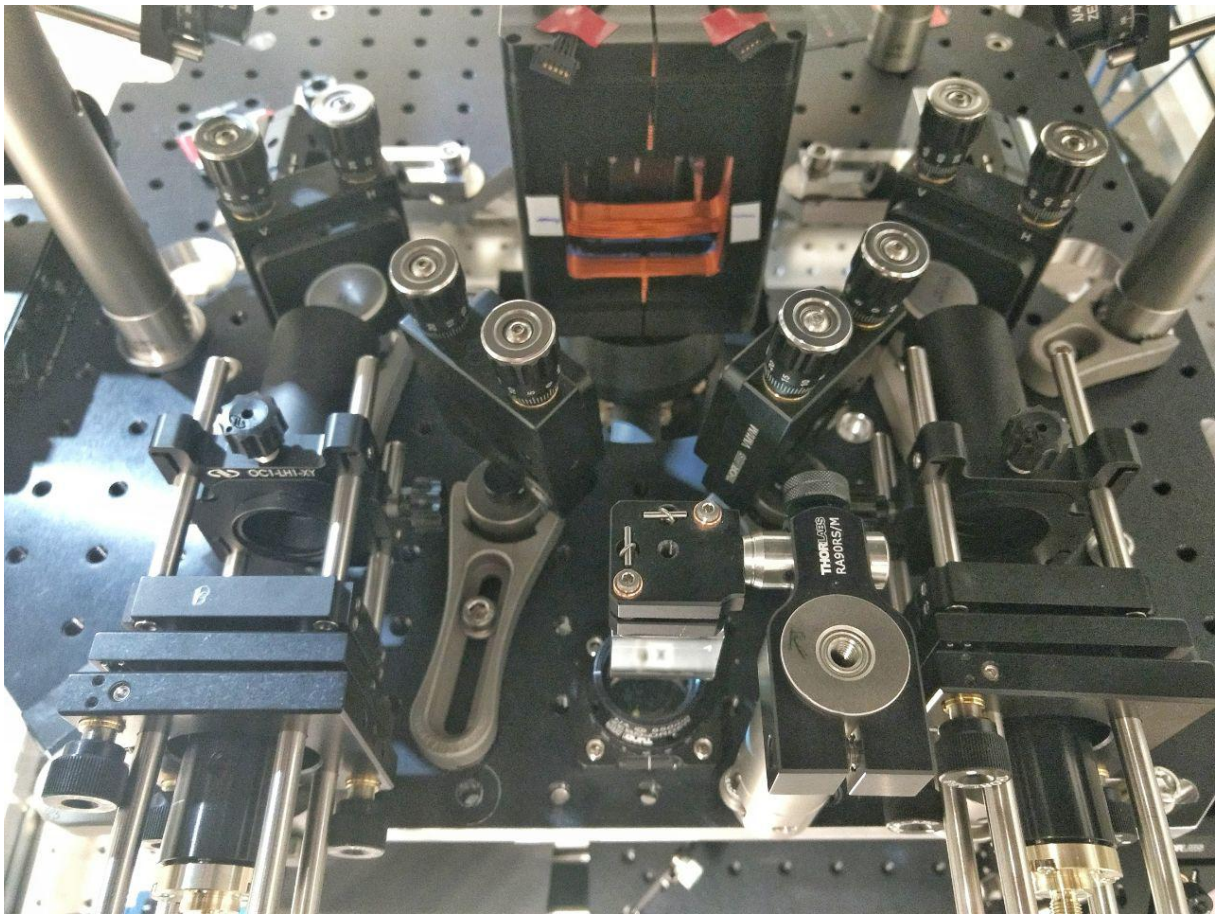

Figure 3.4: Photo of the laser setup near the chip.

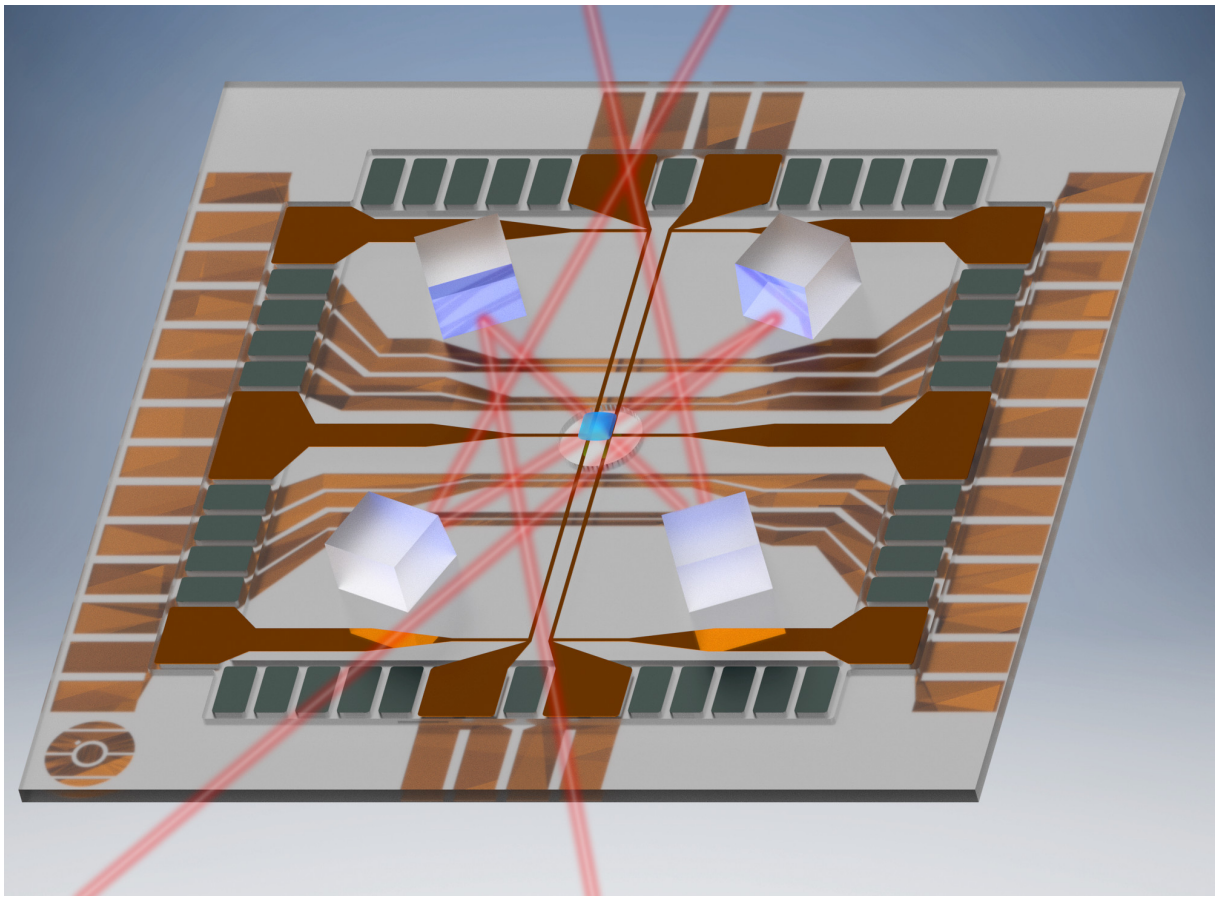

Figure 3.5: Rendering of the atomchip. The cloudy section of the chip is not transparent in reality, but the clear circle in the middle. The square blocks are the mirrors, each about $2\,\mathrm{mm}$ by $2\,\mathrm{mm}$ large and angled. Two beams hitting the mirrors under a certain angle will cross orthogonally in the middle of the chip

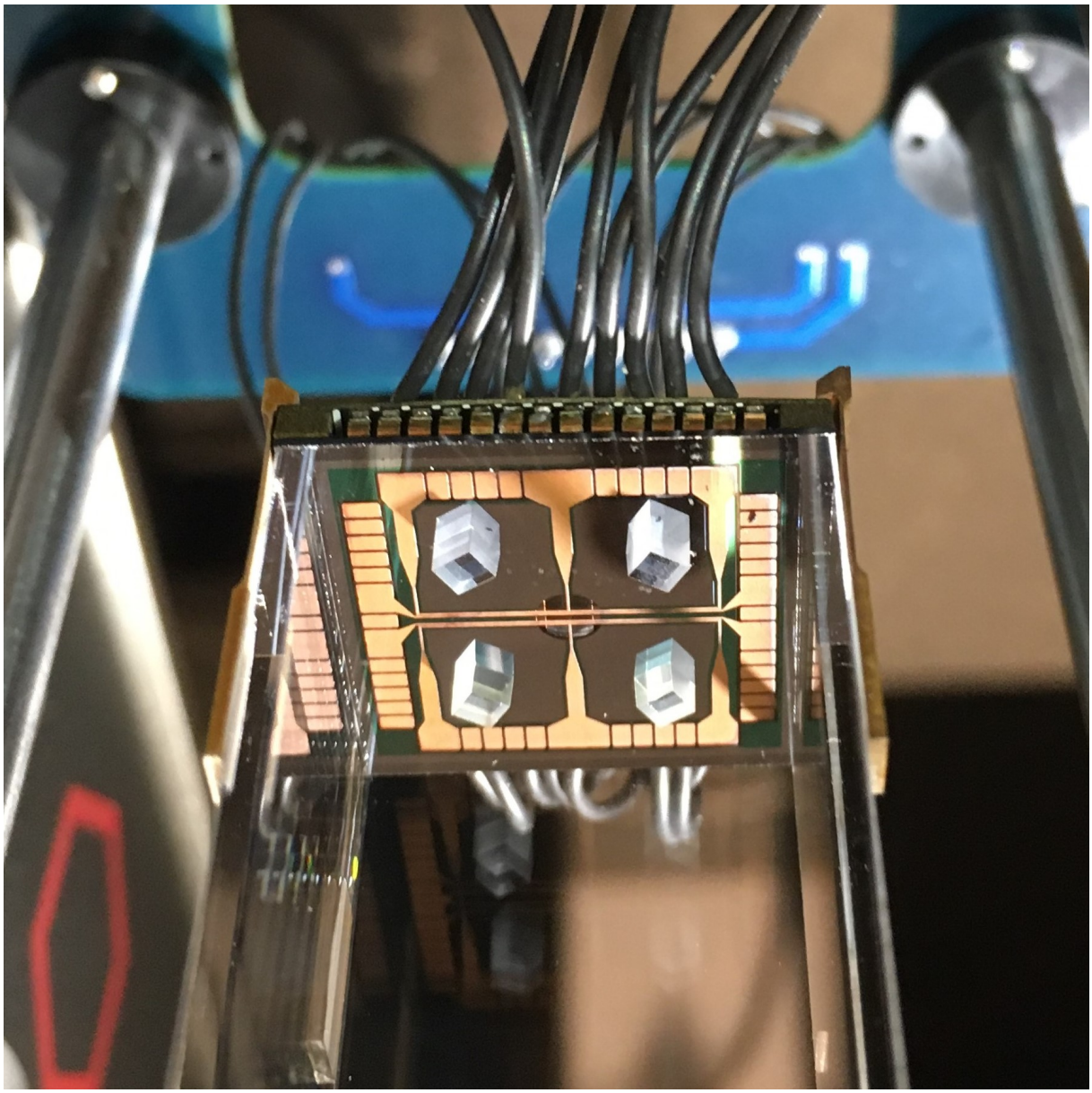

Figure 3.6: Photo of the atomchip.

3.2 Fibres and couplers

The glass fibres used in our experiment are so-called *single mode polarization maintaining fibres*. A typical optical fibre consists of a transparent core surrounded by a transparent cladding with a lower index of refraction. In a multi mode fibre the light inside the fibre always hits the boundary between core and cladding at an angle smaller tan the critical angle given by

$$\Theta_c = arcsin(\frac{n_{core}}{n_{clad}}) \tag{3.1}$$

and is therefore always totally reflected. This phenomenon is called *total internal reflection*. If the diameter of the core is made so thin as to prohibit any mode that is not the fundamental from entering it is called a single mode fibre. It serves as a wave guide for light of a certain wavelength matching the lowest single mode. The required diameter at which this happens has to be found by solving Maxwell's equations with the fibres boundary conditions [12]. Generally it can be said, that the fibres core is at its maximum a few multiples of the wavelength with typical core diameters between 8 and 10.5 µm for a wavelength of 1064 nm.

If the core of the fibre is stressed by placing two rods in the cladding on opposite sides of the core the refractive index can be made dependent on the polarization because the core is stretched in one and compressed in the other direction (stress birefringence). We now have two distinct polarization modes in the fibre. If an incoming beams polarization is aligned with one of the fibres modes then the polarization will be maintained.

To couple a beam with diameter b into a fibre it has to be focussed by a lens to a spot size smaller than the fibres core diameter d and be aligned to hit the fibres core in the center. Another important restriction is, that the numerical aperture of the lens must be equal to that of the fibre. The numerical aperture is given by

$$\mathrm{NA} = nsin(\Theta)\,. \tag{3.2}$$

Since both the fibre and the coupling optics are made of glass and therefore have very similar refraction

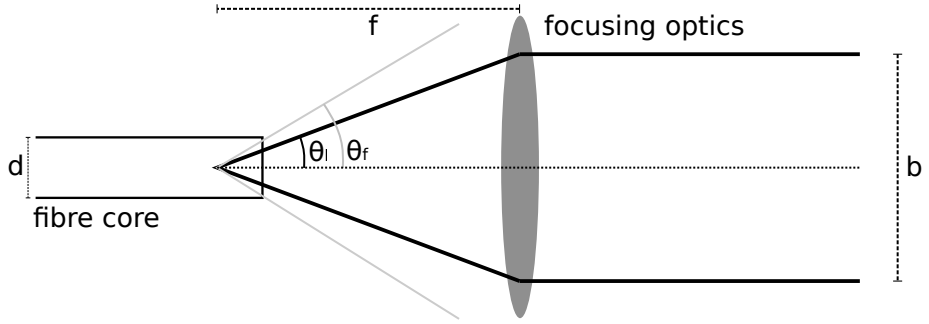

Figure 3.7: A beam with diameter b is focussed to a spotsize smaller than the cores diameter d by a lens with focal length f. For highest coupling efficiencies the lenses focussing angle Θ_l should be equal to the angle under which the light would leave the fibre Θ_f.

indices n this can be understood as the requirement, that the focusing angle Θ_l of the lens is equal to the angle under which the light would leave the fibre Θ_f. This is illustrated in figure 3.7.

Based on these parameters we chose "NKT aeroGUIDE-Power" fibres and "Schäfter Kirchoff 60FC-SMA-T-23-A11-03" and "60FC-SMA-T-23-M35-03" fibre couplers. The "A11" type is used for coupling the 1.2 mm diameter laser beam into the fibre. The "M35" type is used for coupling the beam out of the fibre on the experiment side. The output beam with a waist of 1.6 mm together with the 25 cm focal length lens achieves the proper waist size of 50 µm in the trap.

3.3 The laser

The laser we are using is a "Azure Light Systems" continuous wave *MOPA* (master oscillator power amplifier) laser with a wavelength of 1064 nm and a maximum output power of 50 W.

It uses an ytterbium doped fibre to amplify the output of a 1064 nm seeding laser. Typically fibres used for such an application this are so-called *double clad fibres*. They consist of a core doped with a rare-earth element and two cladding layers. The choice of element depends on the wavelength one wants to achieve. The first cladding layer has a lower index of refraction than the core guiding the laser light as discussed in section 3.2. The outer cladding again has a lower index of refraction than the inner one. This allows to couple pumping light into the inner cladding that then can also pass into the core, amplifying the laser inside. In contrast to normal optical fibres the claddings are typically not concentric and sometimes not even circular to increase

the overlap of the pumping lights modes with the doped core to increase efficiency.

The use of fibres for laser amplification allows for large amplification areas because the fibres can be made long and coiled up. They are also easily cooled because of their large surface area. Both of these facts allow for very high output powers.

Our specific laser uses two such amplification stages one with one pump diode and the other with two. Optical isolators are placed between all stages of the laser and in the laser head. An optical isolator is a component that uses the Faraday effect to allow polarized light to pass only in one direction and not the other. They are used to reduce damaging optical feedback into the different stages of the laser.

The data sheet of the laser claims the wavelength to be 1064 ± 5 nm, the power instability to be smaller than 3% per 8 hours, the maximum output power to be 48 W and the beams M^2 value to be smaller than 1.1. While the first three claims were proven correct the last one was not, as we will see in the next chapter.

3.4 AOMs

We use "IntraAction ATM-802DA2" high power AOMs with "IntraAction ME-803-6" drivers that can output up to 3W of driving power. The AOMs are used to shift the frequency of the two laser beams up and down by 80 MHz respectively and to tune their power. When properly aligned and the driver power at 3 W, the AOMs first or minus-first order yield is around 90%. The beams were not focussed, but left at their original 1.2 mm beam diameter. When this much RF power is used, the AOMs heat up to about 40 °C in around 20 minutes. Because it did not seem like they had reached thermal equilibrium yet and were bound to further increase their temperature, we implemented a solution for cooling the AOMs. To mitigate the heating of the AOMs we designed copper blocks on which we could mount the AOMs using screws (this can be seen in figure 3.2). Good thermal contact was assured by using a drop of thermal paste. The copper blocks act as large thermal mass that the AOMs are coupled to, stabilising their temperature, and dissipating heat due to their large surface area compared to the AOMs alone. When testing the AOMs at full power after being mounted on the blocks the time it took for them to reach 40 °C degrees increased to about one hour and even after two

hours the temperature did not exceed 42 °C

3.5 Safety

Although wearing laser safety glasses is mandatory when the laser is switched on we also decided to enclose the optical setup. For this I designed and built a laser proof box from aluminium profiles and laser proof plates. The box also serves the secondary purpose to keep dust away from the optical components. This is not only important for ensuring beam quality but also to protect the optical components from damage. A small dust particle on the surface of, for example, a mirror would be heated by a high power laser beam enough to be burned right into the mirrors surface, thus ruining it.

I also designed a railing for the main laser setup. It protects the setup from being misaligned if someone accidentally bumps into the optical table and ads an extra layer of protection against stray laser beams. The railing is about 15 cm high with a gap of 3 cm at the bottom to ensure the laminar airflow from the air conditioning is not disturbed.

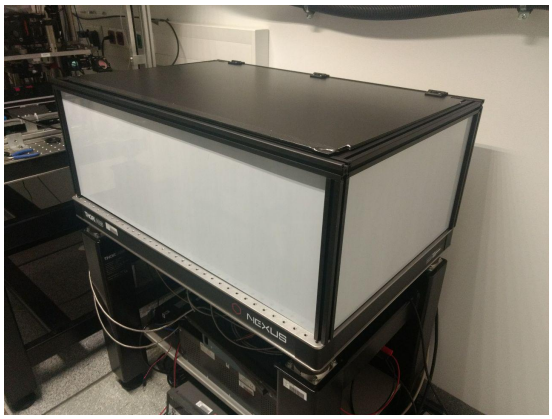

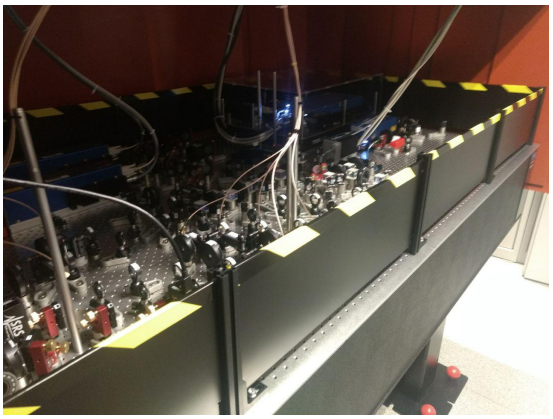

Figure 3.8: Pictures of the box protecting the dipole setup and the railing for the big laser table

und als man es merkte,

da war's schon zu spätchen.

4

Characterization

With the setup built I characterized the beams quality and power stability.

4.1 Power measurements

To characterize the setup, I measured the efficiencies of all the optical components that are expected to be lossy. The values can be found in table 4.1. Furthermore we tested the functionality of the experiment sided part of the setup by aligning the beam such that it hits the mirrors on the atomchip. Using a USB camera pointed at the atomchip, so we could see the beam hitting the mirrors, made this surprisingly easy. We then tested if the mirrors would withstand the high laser powers. This was done by slowly ramping up the laser power up to 5 W and monitoring the out-coming beams position. If the out-coming beam would have moved

Efficiency	Component
85%	Pinhole filter
90%	AOMs ± 1
87%	Fibre Couplers

Table 4.1: Efficiencies of the lossy optical components

we would have known, that the mirrors were warping because of thermal stress. Luckily we did not see any such effects.

4.2 Beam quality

Before building the setup I characterized the laser beam quality by measuring its M^2 value. I did this by placing the 25 cm focal length lens, that will be used for focusing the beam for the trap, right after the laser head and measuring the beam diameter at every cm after the lens. This was done by mounting our beam profiler on a rectangular post and sliding it along an aluminium profile with a ruler attached to it. This was an efficient way to do the measurement and the placement precision of about ± 0.5 mm was sufficient. After measuring the waist size in the region twice the focal length behind the lens I fitted the following function to the data.

$$w(z) = w_0 \left(1 + M^2 (\frac{\lambda(z - Z_0)}{\pi w_0^2})^2\right)^{1/2} . \tag{4.1}$$

Equation 4.1 is very similar to 1.18, the only differences being the two added fit parameters, namely the factor M^2 that describes the deviation of the beam intensity profile curve from the one of a perfectly Gaussian beam and the constant Z_0 that translates the function along the z axis to adjust the fit if the focus is not perfectly at center.

The M^2 value characterizes the difference between the measured beam and an ideal Gaussian one. A beam with with $M^2 = 1$ is perfectly Gaussian and a M^2 value larger than one quantifies the deviation from a purely Gaussian mode.

The measurement for the beam straight out of the laser head is shown in figure 4.1, and two pictures of

the beam profile at different distances after the lens are shown in figure 4.2. As can be seen by the measurement of the waist size and the speckle patter in Figure 4.2b the beam is non-Gaussian, to the extent that the fit function centred around $z - Z_0 = 0$ does not capture the beam profile. This was because the fit function is symmetric around $z - Z_0 = 0$ whereas the data was not. This asymmetry may stem from the fact, that the beam profiler measures beam diameter by fitting a function to the image of the beam that is not compatible with the speckle pattern seen in figure 4.2b. To check if my measurement was at fault (for example the lens having some defects), and to test our fibre couplers, I redid the measurement with the beam coming out of or high power single mode fibre via a fibre coupler. Since you can only couple the Gaussian mode into the fibre I expected to see an almost perfectly Gaussian beam coming out of the fibre. This measurement can be seen in 4.3. As you can see this time the beam is, as expected, almost perfectly Gaussian with a $M^2 = 1.047$. Since this measurement was done with the exact same setup as the first one I was now confident, that the first measurement was also correct. This measurement also confirmed, that the beam directed to the atomchip would be focused to the desired waist size without loosing quality, with the waist size measured in the focal point being 54 μm.

The unwanted modes in the laser beam cannot be coupled into the fibre and dissipate at the fibre head and cladding, heat it up, and potentially reduce the fibres lifetime, especially at high powers. To remove any unwanted modes we installed a pinhole filter right after the laserhead. The details of this filter are explained in section 4.3. Our pinhole filter removes about 10% of the beams power and yields an acceptably Gaussian beam profile with $M^2 = 1.15$. This measurement can be seen in figure 4.4.

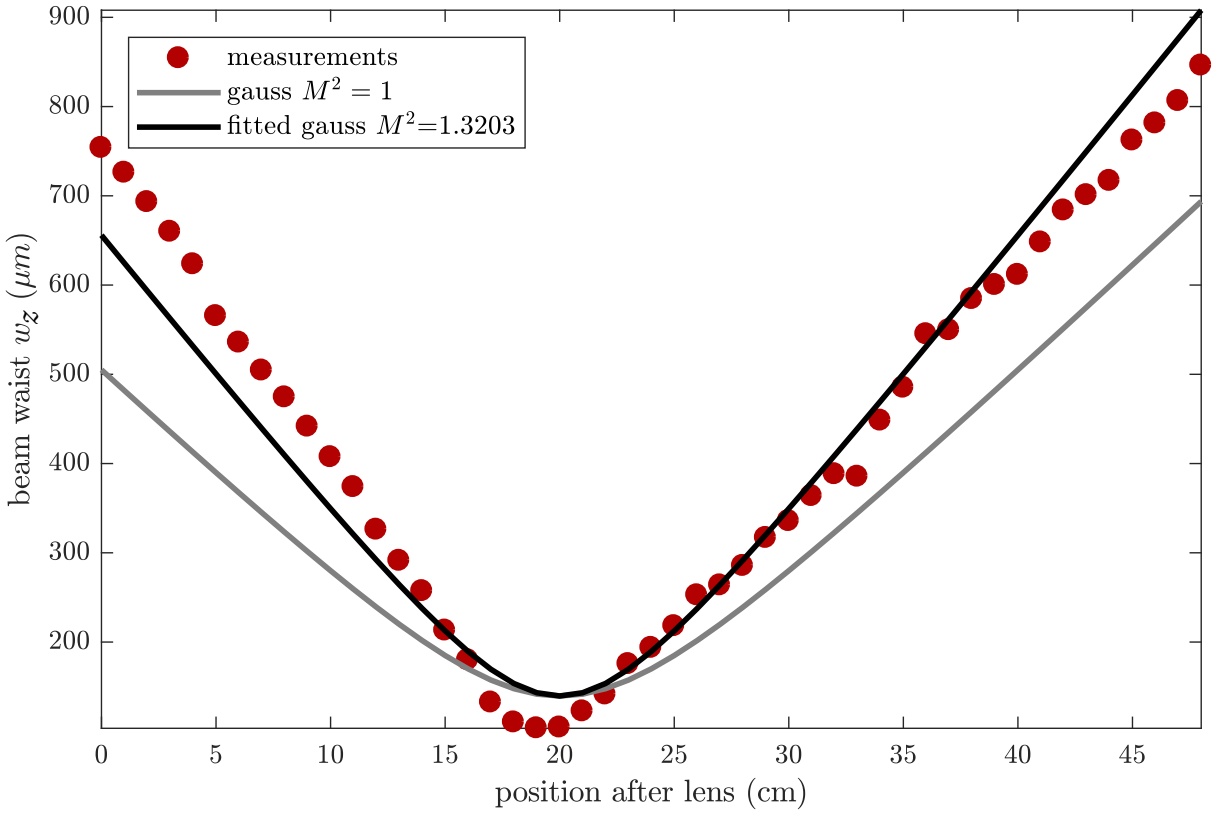

Figure 4.1: M^2 measurement of the beam without any beamshaping after the laserhead. I used a 25 cm focal length lens to focus the beam. As you can see in figure 4.1 the beam was very much not perfectly Gaussian. So much so, that the fit function was not able to fit the data in a satisfactory manner.

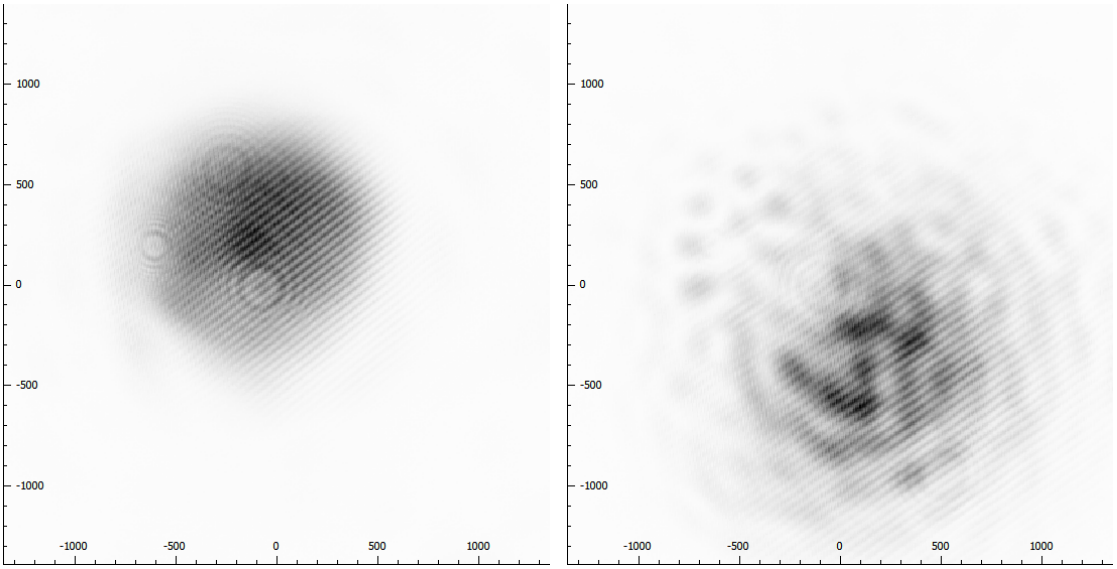

(a) 5 cm after lens

(b) 40 cm after lens

Figure 4.2: Two pictures of the beam profile at different distances after one 25 cm focal length lens. You can see a speckle pattern in 4.2b. It is obvious, that the beam profile is definitely not perfectly Gaussian.

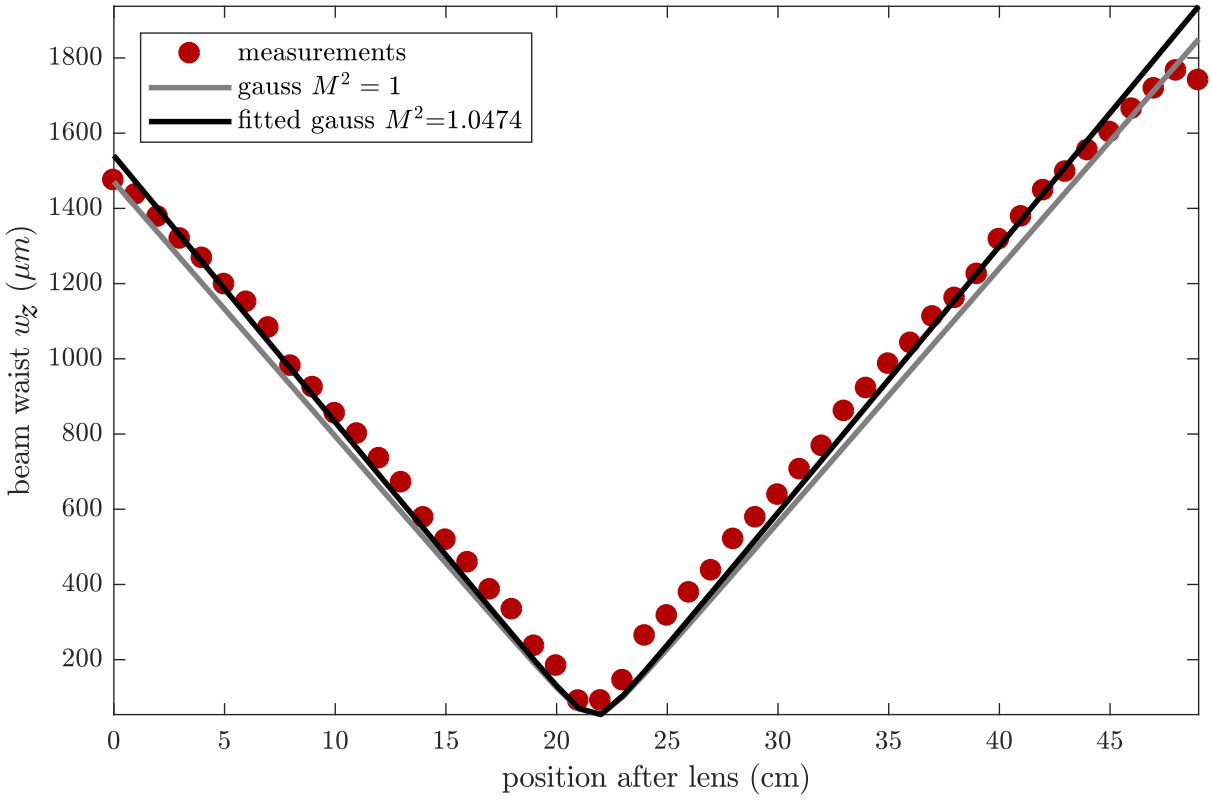

Figure 4.3: Same measurement as in 4.1 but with the laser beam coupled out of a single mode fibre via a M35 fibre coupler. This fibre coupler gives a beam with a diameter of $3.2\,\mathrm{mm}$ compared to the $1.2\,\mathrm{mm}$ used in the other measurements. As you can see the beam is focussed almost like a perfectly Gaussian one. This tells us, that in the measurement before the laser is at fault and not the way of measuring.

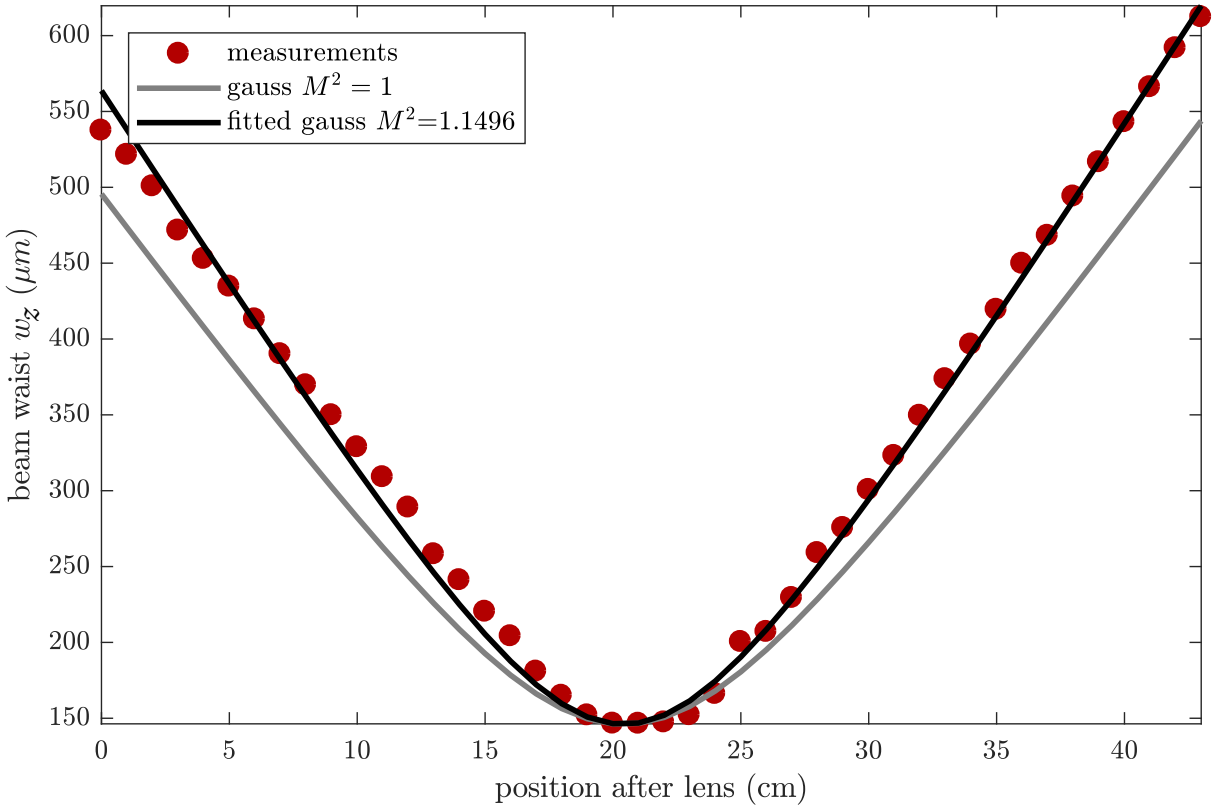

Figure 4.4: Again the same measurement but now the unwanted modes are filtered out by a pinhole filter. This greatly improved beam quality.

4.3 Pinhole filter

As mentioned in the previous section we needed to remove non-Gaussian modes from our laser beam. To do this we choose to use a so-called pinhole filter. When a Gaussian beam is focused, the smallest achievable spot size with a diffraction limited lens of a given focal length is given by the diffraction-limited spot diameter

$$D = \frac{\lambda f}{d}, \tag{4.2}$$

where f is the focal length and d the diameter of the beam before the lens. The spot diameter relates to the minimum waist size by $D = 2w_0$. The Gaussian mode is the only mode , that can be focused to this spot size. From a spot size larger than D one can infer, that the beam used was not perfectly Gaussian. You now aim the beam through a small pinhole that has a diameter just a bit larger than the spot size. Doing this will only allow the most focused, Gaussian, mode to pass through. The rest will be absorbed by the material around the hole.

A pinhole like this has to be very round and thin and needs to be able to withstand a highly focused high power laser beam. We could choose between three high power pinholes with 10 μm, 25 μm or 50 μm. The manufacturer of these recommends* to use a pinhole 30% larger than the diffraction limited waist size. Calculating the needed focal length for each hole size and our beam diameter of 1.2 mm and comparing with which aspheric† lenses were available we decided that a 11 mm lens would fit best. This lens focuses the beam to a 19.51 μm diffraction limited spot which gives a pinhole size of $P = 1.3D = 25.36$ μm. Also it allows us to build a compact filter without the lens being to close to the filter, which would make the pinhole assembly harder to build.

The final assembly as seen in figure 3.2 on the right consists of a precision xy-stage in which the pinhole is mounted. The xy stage is used to center the pinhole. Onto the xy-stage I mounted two z-stages using cage rods. The first in front of the pinhole and the second after the pinhole. The first z stage is used to precisely

*https://www.thorlabs.com/thorproduct.cfm?partnumber=P25C

†Aspheric lenses are lenses with a more optimized, non-spherical lens shape than simple lenses, reducing spherical and other aberations.

place the focal point of a 11 mm aspheric lens right in the center of the pinhole. The second z-stage moves the same type of lens and is used to collimate the beam again.

To align the beam with the pinhole I removed both lenses and the pinhole from the assembly. Then I attached two irises in place of the lenses and measured power after the second iris. I closed the irises to a minimal aperture without completely loosing signal and adjusted the beam using two mirrors until I reached maximum intensity, closing the irises further and repeating, until I was sure, that the beam passed straight through the assembly. Afterwards I mounted the pinhole in the xy-stage, making sure that the stage was in a centred position and opened the first iris so that more light would hit the front of the pinhole. Since the pinhole only allows a small amount of light to pass through if the beam is not focused I also increased the laser power to around 200 mW to get more signal at the power meter. Then I moved the pinhole in the xy-stage to further increase to a new maximum. After that I again closed the irises further and repeated the other steps until the beam was perfectly aimed through both almost closed irises and the pinhole. Then I replaced the first iris with the z-stage and lens, removed the second iris and moved the power meter head as close as possible to the back of the pinhole since the beam would be very defocused after the first lens. I made sure, that the z-stage was set so that it had about equal amount of travel in both directions and mounted it so that the lens was about 11 mm away from the pinhole. To center the focal point of the lens into the pinhole I first adjusted the z-stage for maximum power then the xy-stage and finally and very carefully tested if adjusting the mirrors could further improve the alignment. After repeating this for a few times, until no further improvement was noticeable, I mounted the second z-stage with the lens and adjusted it so that the beam was properly collimated. I checked collimation by moving a beam viewer along the beam, if there were no focal points along the way I placed the beam profiler as far away as possible and fine adjusted the z-stage until the beam had the desired diameter of 1.2 mm.

The aligned filter removes about 15% of beam power and improved the fibre coupling efficiencies that I could achieve from 45% to almost 90%.

4.4 Power stability

To test the power stability of our laser I measured the power over a few hours noticing, that the power would increase in regular intervals. After spending some time in the lab we noticed sudden temperature drops at regular intervals and started to simultaneously measure laser power right after the laser head and the temperature in the room, using two low thermal mass thermocouples at different places in the room. This plot can be seen in figure 4.5. As can be seen in the plot the air-conditioning lowers the temperature in the room by around 3 °C every half hour, causing an increase in laser power by about 100 mW. The sudden drop in temperature happens because of two reasons: firstly the air-conditioning is a bit to powerful for the small room it is in and secondly the temperature sensor controlling the air conditioning has relatively high thermal mass so the temperature control circuit does not even notice the sudden drop in temperature. Tweaking the air-conditioning is non-trivial and still ongoing. The rise in laser power can either stem from the main laser unit or from the laser head mounted on the optical table. We later build a box around the whole set-up for laser safety reasons (more on that in 3.5) and in the hope it would reduce the power fluctuations; sadly it did not. This tells us, that the fluctuations come mainly from the main laser unit and not the laser head mounted on the table, nor the components in the optical setup (for example polarizing beam splitters). On a more positive note, the laser showed long term drift of less than 10 mW over a timespan of eight hours.

Another way to mediate the power fluctuations is to measure the beam power before coupling into the fibres by reflecting only a tiny amount of power out of the beam using a glass plate. Then use the AOM drivers amplitude modulation feature together with a active feedback circuit to compensate for the fluctuations. This is planned to be a future project.

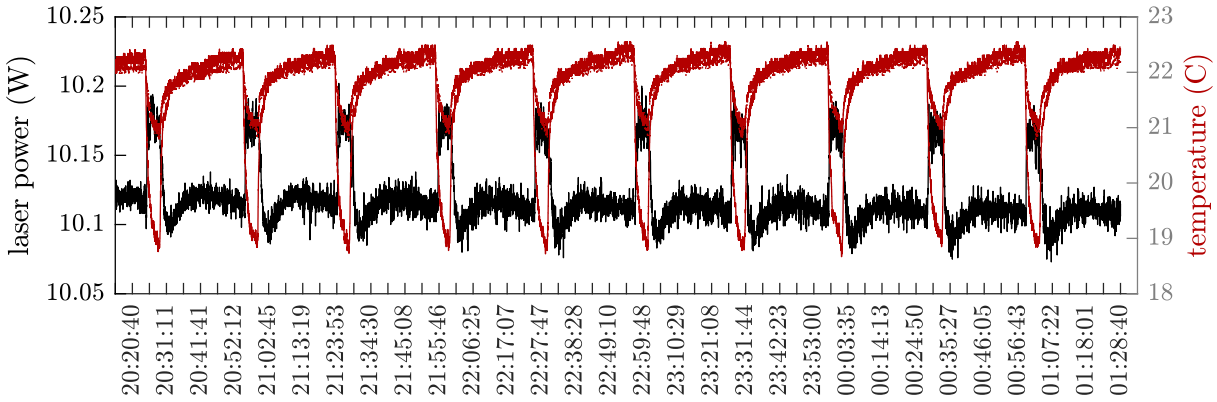

Figure 4.5: This plot shows the correlation between laser power and the temperature in the lab without a box around it.

4.5 AOM Calibration

The AOM-Drivers can be amplitude modulate by applying a voltage to its AM input. To make this more user-friendly in our control software we made a calibration measurement that enables us to set power percentages instead of voltages. We ramped the control voltage linearly form 0 V to 10 V corresponding to 0 W to 3 W in 60 ms and measured the laser power in the first order beam. This measurement was repeated for two hours and all measurements were averaged to remove the impact of the temperature fluctuations changing the laser power (see figure 4.6).

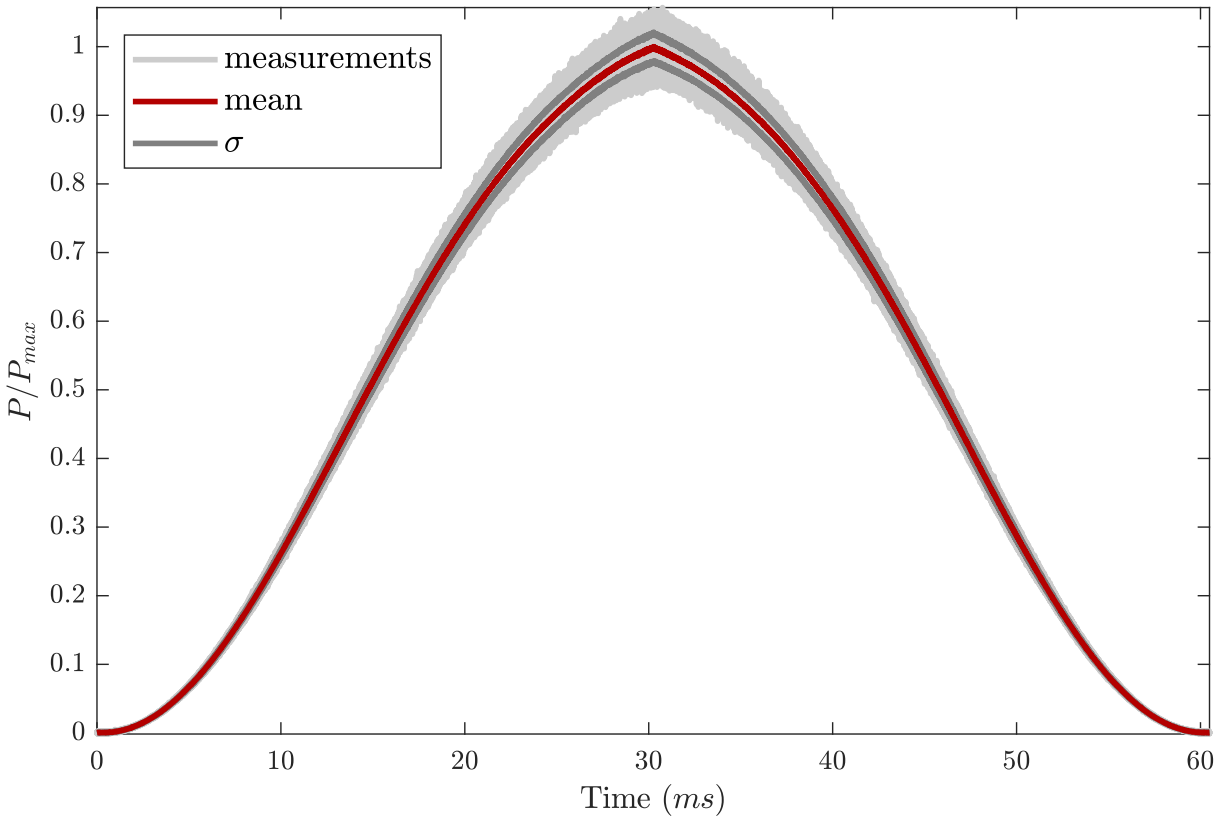

(a) All measurements (plotted in grey) were averaged to give the mean calibration cruve (red) with the one sigma confidence bounds shown in dark grey.

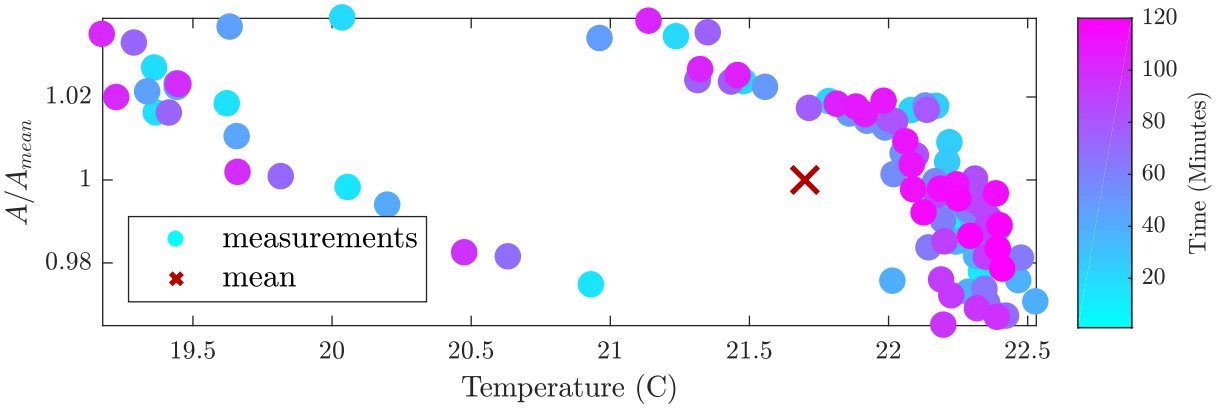

(b) Statistics for calibration measurement: to get a feeling for the variation in the measurement I plotted the normalized integral of each curve against the temperature in the room. The red marker marks the mean curve the other measurements are plotted as dots with colour correlating to the time the measurement was taken.

Figure 4.6: AOM Calibration

Da war der Metterschling schon feit wort...

wanz geit...

Mit lut er teid.

Mira Lobe

5

Loading atoms

In this chapter I will give a overview of the full experiment up to the point of the atoms being trapped in the dipole trap. The core of the experiment is a glass chamber in the shape of a square hourglass. The chamber is about 20 cm high and 3 cm wide. It is evacuated to 10^{-11} mbar and the the vacuum is maintained by an ion pump. A caesium dispenser in the bottom of the chamber is heated by applying a current of 2.5 A and some atoms evaporate. The atoms are then collected in a line on the z-axis by a two-dimensional magneto-optical trap and then pushed through the hole in the middle of the glass chamber to the other side. There they are trapped and cooled by a three-dimensional magneto-optical trap. The resulting cloud of atoms is, after further cooling in a short molasses phase, optically pumped in a magnetically trappable state and loaded into a magnetic trap. From there the atoms are loaded into a chip trap and then into the dipole trap where

they are cooled by evaporative cooling until a Bose-Einstein-Condensate eventually forms.

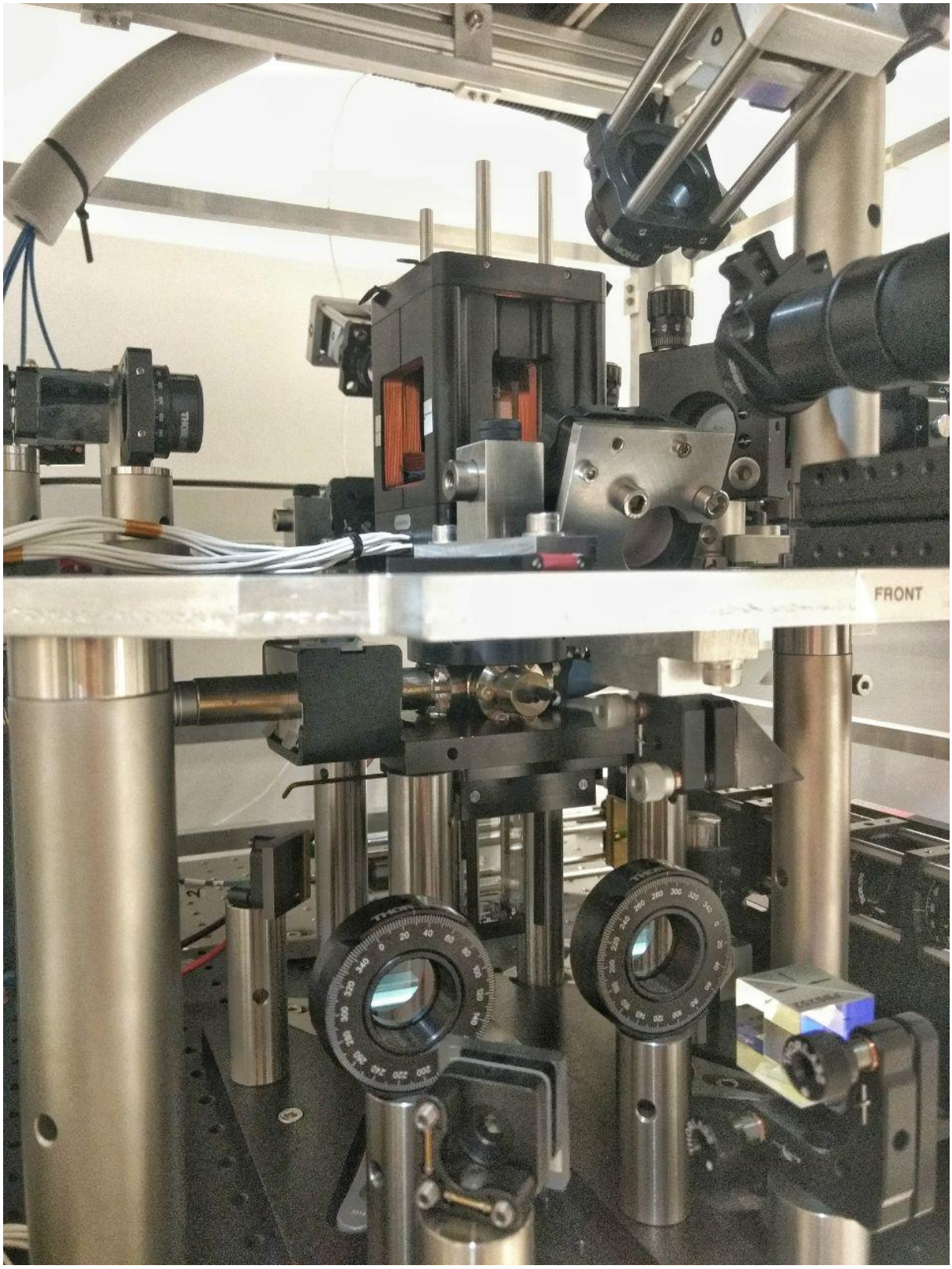

Figure 5.1: Photo of the Experiment. In the lower half you can see the PBS for the 2D MOT, the two $\lambda/4$ plates used for adjusting the polarization and the lower part of the glass chamber surounded by the magnetic rods. Also the ion pump attached to the middle of the glass chamber. In the second half of the photo the coils surrounding the upper half of the glass chamber are visible.

5.1 Magneto optical trapping and laser cooling

Here I will give a short introduction to the theory behind magneto-optical traps and laser cooling. My treatment will follow that in "Atomic physics" by C.J. Foot[13].

A magneto-optical trap (MOT) consists of three orthogonal pairs of counter propagating, circularly polarized laser beams and a pair of coils in an anti-Helmholtz configuration. The beams are tuned to be just below the atomic resonance. When the atom has a velocity v, along the axis of a beam, the Doppler shift moves the laser light closer to resonance, therefore increasing the probability of scattering a photon and slowing the atom. This is called optical molasses and is one of the techniques used for laser cooling an cloud of atoms.

The coils produce a quadrupole magnetic field with its minimum of $B = 0$ at the point where the laser beams intersect. Close to the minimum the magnetic field increases linearly in every direction. This causes a Zeeman-shift of the atomic transition moving it closer to being in resonance with the laser beams light propagating in the opposite direction. Resulting in a restoring force that "pulls" atoms back into the middle of the trap.

5.2 Setting up the 2D magneto optical trap

Next to the lower half of our glass chamber four magnetic rods are mounted. The field generated by those rods looks like a quadrupole field when viewed from the top but is zero along the whole z axis. The field gradient generated by the rods is $32\,\mathrm{G\,cm^{-1}}$ in one and $28\,\mathrm{G\,cm^{-1}}$ in the other direction [14]. In the region where the field is zero we have to align two elliptically shaped laser beams so that they are orthogonal and their long axis are aligned with the z axis.

The elliptical beams are a mix of two lasers with different wavelength. One laser, responsible for slowing the atoms, is detuned by $-15\,\mathrm{MHz}$ compared to the $D_2(6^2S_{1/2}, F = 4 \rightarrow 6^2P_{1/2}, F = 5)$ transition. It is called the cooler. The other laser, the so-called repumper, is on resonance with the $D_2(6^2S_{1/2}, F = 3 \rightarrow 6^2P_{1/2}, F = 4)$ transition. It serves to recover atoms which fell into the $F = 3$ ground state and would

otherwise be lost. Both lasers are mixed in a ratio of 5/1 cooler to repumper before they are amplified in a laser booster.

The beam shaping is done by a ”telescope” consisting of one spherical and two cylindrical lenses. Both cylindrical lenses are mounted in rotational mounts. To get a beam which neither converges nor diverges in any of its axis we spent quite some time adjusting this telescope setup. For adjusting we used a mirror placed right after the ”telescope” and reflected the beam out of the setup and onto a wall about two meters away. We then set the all the lens distances to the configuration that was given by the manufacturer knowing that it was meant for a different wavelength. From there we adjusted the distances and positions until the beam was about 3 cm high and 5 mm wide and we could move a beam viewer card along the whole two meters without seeing any change in beam shape.

After the lens setup the beam is split by a beam splitter and one part aligned along the x and one along the y axis. Each beam is then reflected back by a mirror after passing trough a $\lambda/4$ plate. Since we could access the point in which the beams crossed, the glass chamber was in the way, we had to find another way of aligning the two beams with the center of the chamber.

Below the glass chamber a mirror is mounted that reflects a laser beam upwards to push the atoms in the 2D MOT up and through a hole serving as differential pumping stage to the upper part of the chamber. This beam is called the push-beam. We first aligned the mirror so that the beam hit the hole and the middle of the glass chambers ”ceiling”. Then we blocked both the elliptical and push-beam with a plate with a small hole in its middle. We now tuned the laser light to our atomic resonance and turned on the Cs dispenser. The Cs atoms in the chamber would now scatter light when moving into the laser beams. With a USB camera without infra-red filter we were now able to see all three beams as thin lines in the chamber due to resonant fluorescence. We were now able to align the two elliptical beams with the push-beam and adjust the retro reflecting mirrors so that the beams would be perfectly reflected into themselves. To further improve alignment we turned of the push-beam and placed a camera with a focusing lens in front pointed at the mirror below the chamber. We then focused the camera on the hole to the upper part of the chamber. We now could see two

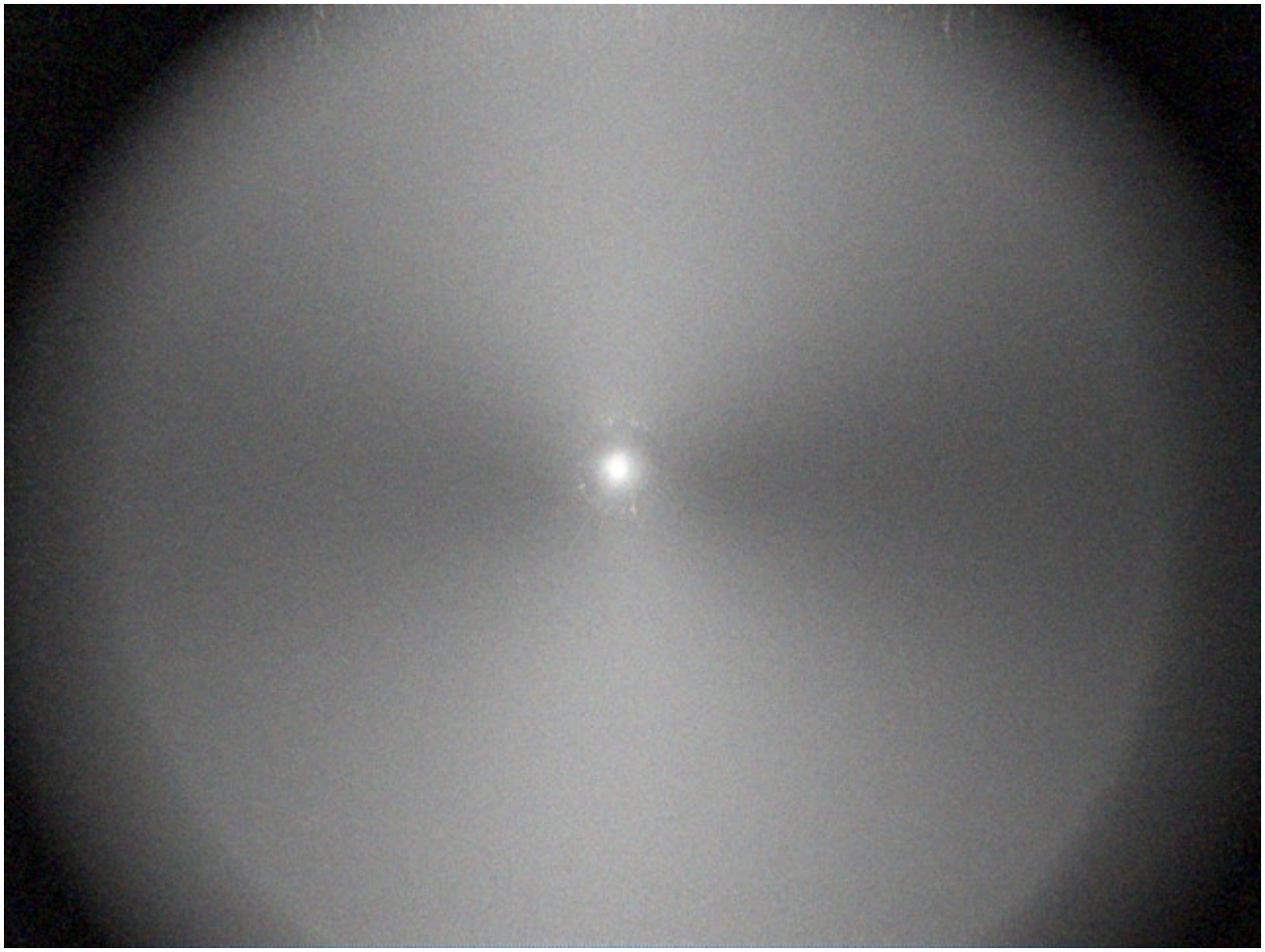

Figure 5.2: Picture taken of the 2D MOT from below. The circular shape tells us, that the line of atoms lies exactly on the axis of the camera. The gradient in the background is due to the magnetic field present. Stray light is scattered more by atoms that had their atomic resoance shifted towards the lights frequency. The fact, that the gradient lines cross in the middle tells us, that the magnets are porperly adjusted. The faint ring visible around the atom cloud is the hole leading to the upper chaber and has a diameter of $750\,\mu\mathrm{m}$. The intensity per beam was $11.4\,\mathrm{mW/cm^2}$.

faint lines crossing in front of the hole indicating proper alignment of the 2D MOT. To test it we again detuned the laser by -15 MHz compared to the resonance and watched a bright spot form on the images taken by the camera right in front of the hole. This told us, that a line of cold atoms had formed and that it was perfectly aligned with the z axis, otherwise we would not see it as a spot from below. When the push-beam would now be turned on we would push atoms up into the upper half of our experiment to be captured by the 3D MOT.

5.3 Setting up the 3D magneto optical trap

The 3D MOT in our experiment is built exactly like I described at the start of this chapter with two exceptions. Firstly the counter propagating beams are a mixture of two lasers with different wavelengths as in the 2D MOT. Secondly two of the beams are not perfectly orthogonal but cross under a angle of 44°. This is due to the space restraints in our setup.

The beams have a diameter of about 2 cm which is about the same size as the mirrors used to align the beams. This made it harder to align everything since it was not enough to check if the centres of the beams properly crossed but also if none of the beams were cut of at any point. These space restraints also made the alignment of the 3D MOT a bit harder then it would normally have been. Because of space restrictions we had to rethink the design of the setup twice. We pre-adjusted the MOT setup detached from the main experiment using a red laser coupled into the fibres that would later be used for the infra-red laser. This way we could adjust all the mirrors with visible light and also align the beams so that they cross right where the middle of the glass chamber was going to be when the setup was built into the experiment. We also measured all the polarizations and set the $\lambda/4$-wave-plates to polarize our beams circularly. Afterwards we checked the wave front of all the beams with a shear plate because we saw a change in the form of the red lasers beam profile when changing its polarization before a polarizing beam splitter. After some investigation it turned out that the second mirror in the beams path was faulty. Exchanging it misaligned all the beams slightly, forcing us to readjust everything again. When everything was aligned again we attached the setup to our experiment.

Doing that we found out, that although it was easier to align everything away from the experiment, saving us some work, it did not pay of in the end since the setup slightly misaligned while we carried it from one optical table to the next. I goes without saying, that we then readjusted yet again, of course having a harder time adjusting since the point where the beams crossed was not accessible any more.

After aligning we started to build a rack that would hold all the power supplies and electronics needed to run the experiment, mounted said power supplies in the rack, estimated that the fuse of the wall plug would blow when all power supplies were turned on (this was later fixed by the institutes electrician) and started to test and characterize them in combination with our control software.

With the power supplies operational we connected them to the coils producing the magnetic field for the MOT. After making sure that their temperature stayed reasonable when we used the maximum rated current, we tried to trap some atoms. With the 2D MOT and the push-beam turned on we adjusted the strength of the magnetic field to a field gradient of 13.5 G cm^{-1} and the beams until the MOT appeared as a white spot on our cameras.

At the time of writing, this is as far as we got. The rest of this chapter will now detail what is planed to come next, up to the point where atoms are finally loaded into the dipole trap.

5.4 Further experimental cycle

As explained in the introduction to this chapter, the atoms are Doppler-cooled while in the MOT. After the cloud is sufficiently cold, the magnetic fields are turned of and the lasers will be further detuned (around -60 MHz) to further cool them to temperatures below what could be achieved with Doppler cooling. The exact mechanisms by which this happens are beyond the scope of this thesis. But I will quote what J. Foot [13] says (only in a footnote) about this kind of optical molasses:

> In real optical molasses experiments, the three mutually-orthogonal pairs of laser beams create a complex threedimensional pattern of polarization and a combination of sub-Doppler cooling mechanisms takes place.

This phase can only last for up to 10 ms, otherwise the, now no longer confined, atoms would just fall

down. Afterwards a homogenious magentic field along the z axis is turned on, so that the atoms can have a defined m_f state. Now the atoms are optically pumped into a low-field seeking state, which is also a dark state with respect to the wavelength of the pump beam. A low field seeking state is a state where the gyro magnetic factor g_f and m_f are both either positive or negative, since the strength of interaction with the magetic field is proportional to their product. Dark state means, that once the atoms is in its new state it will not interact with the pump beam any more. If the atoms would still interact with the pump beam the cloud would be heated again. The state we want our atoms to be in is the $6^2S_{1/2}, F = 4, m_f = 4$ state with $g_f = 0.35\,\mathrm{MHz\,G^{-1}}$. To achieve this, the pump beam is tuned to the $D_2(6^2S_{1/2}, F = 4 \rightarrow 6^2P_{1/2}, F = 4)$ transition and circularly polarized (m_f states can be ignored since the magnetic field is weak and the splitting between m_f states therefore is very small). Every time a atom is excited its m_f value increases because of the selection rules for circularly polarised light and it relaxes back to the $F = 4$ ground state, but with increased m_f. When $m_f = 4$ is reached the atom cannot be excited any more since the $F = 4$ excited state cant have a $m_f = 5$, thus the sate is now "dark" to the pump beam. Since the atoms have a certain probability of also relaxing into the $F = 3$ ground state a so called repumping beam, tuned to the $F = 3 \rightarrow F = 4$ transition in mixed into the pump beam. This is done because those atoms would otherwise be lost. This phase also takes about 1 ms

Now that the atoms are in a magnetically trappable low field seeking state we again turn on our anti Helmholtz coils to produce a quadrupole field with $B = 0$ in its centre. The field is the same as in the MOT but with a stronger gradient. With another pair of other coils we can now adiabatically deform the trap so that the $B = 0$ region moves up until we are a few millimetres away from the atom chip. On the side of the atomchip facing the inside of the chamber straight PCB tracks can generate a magnetic field that also traps our atoms. We now switch of the magnetic trap and simultaneously switch on the chip trap in such a way that the cloud of atoms wont get heated to much. Now we us a microwave antenna, that is mounted outside the glass chamber on top of the atom chip to pump the atoms from the $F = 4, m_f = 4$ ground state to the $F = 3, m_f = 3$ ground state. This state now is a high field seeker and therefore not magnetically trappable and we finally turn on the dipole

trap and create a BEC by weakening the dipole trap and therefore cooling the cloud of atoms by evaporative cooling.

6

Conclusion

The setup for generating and modulating the laser beams to be used for the dipole trap is finished and characterized. It achieves higher efficiencies than expected and can be easily controlled via our control software. The experiment side of the setup yields sufficient beam quality and can be aligned with relative ease. We also proved, that the mirrors on the atomchip can withstand the high laser powers we want to use.

In theory the trap should be able to achieve all the goals we set out for it to achieve. However because of some delays in the other parts of the experiment the trap was never tested with atoms in it. This work will mark the beginning of my PhD on this experiment.

References

[1] T. Schumm et al. “Matter-wave interferometry in a double well on an atom chip”. In: *Nature Physics* 1 (Oct. 2005), pp. 57–62. DOI: 10.1038/nphys125. eprint: quant-ph/0507047.

[2] M. H. Anderson et al. “Observation of Bose-Einstein Condensation in a Dilute Atomic Vapor”. In: *Science* (1995).

[3] W. Wing. “On Neutral Particle Trapping in Quasielectrostatic Electromagnetic Fields”. In: *Progress in Quantum Electronics* 8 (1984), p. 181. eprint: physics/9902072.

[4] T. Weber et al. “Three-Body Recombination at Large Scattering Lengths in an Ultracold Atomic Gas”. In: *Physical Review Letters* 91.12, 123201 (Sept. 2003), p. 123201. DOI: 10.1103/PhysRevLett.91.123201. eprint: physics/0304052.

[5] T. Kraemer et al. “Optimized production of a cesium Bose Einstein condensate”. In: *Applied Physics B: Lasers and Optics* 79 (Dec. 2004), pp. 1013–1019. DOI: 10.1007/s00340-004-1657-5. eprint: cond-mat/0408268.

[6] Vladan Vuleti ć et al. “Observation of Low-Field Feshbach Resonances in Collisions of Cesium Atoms”. In: *Phys. Rev. Lett.* 82 (7 Feb. 1999), pp. 1406–1409. DOI: 10.1103/PhysRevLett.82.1406. URL: https://link.aps.org/doi/10.1103/PhysRevLett.82.1406.

[7] T. Weber et al. “Bose-Einstein Condensation of Cesium”. In: *Science* (2003).

[8] R. Grimm, M. Weidemüller, and Y. B. Ovchinnikov. "Optical Dipole Traps for Neutral Atoms". In: *Advances in Atomic Molecular and Optical Physics* 42 (2000), pp. 95–170. DOI: 10.1016/S1049-250X(08)60186-X. eprint: physics/9902072.

[9] *http://raptor.physics.wisc.edu/data/Cs_energy.pdf*. 2018.

[10] Daniel A Steck. *Cesium D line data*. 2003.

[11] Sabine Stock et al. "Observation of Phase Defects in Quasi-2D Bose-Einstein Condensates". In: *Physical review letters* 95 (Dec. 2005), p. 190403. DOI: 10.1103/PhysRevLett.95.190403.

[12] Malvin Carl Teich Bahaa E. A. Saleh. *Fundamentals of Photonics*. Wiley, 2007.

[13] Christopher J. Foot. *Atomic Physics*. Oxford University Press, 2005.

[14] Evan Salim. *Colquanta, Private communication*. 2018.